HHS Public Access

Author manuscript

Nature. Author manuscript; available in PMC 2022 July 01.

Published in final edited form as:

Nature. 2021 July ; 595(7866): 272–277. doi:10.1038/s41586-021-03663-4.

Caloric restriction disrupts the microbiota and colonization resistance

Reiner Jumpertz von Schwartzenberg[1,2,3,&], **Jordan E. Bisanz**[4,&], **Svetlana Lyalina**[5], **Peter Spanogiannopoulos**[4], **Qi Yan Ang**[4], **Jingwei Cai**[6], **Sophia Dickmann**[1], **Marie Friedrich**[1], **Su-Yang Liu**[7], **Stephanie L. Collins**[6], **Danielle Ingebrigtsen**[8], **Steve Miller**[8], **Jessie A. Turnbaugh**[4], **Andrew D. Patterson**[6], **Katherine S. Pollard**[5,9,10], **Knut Mai**[1,2], **Joachim Spranger**[1,2,3,*,+], **Peter J. Turnbaugh**[4,10,*,+]

[1]Charité Universitätsmedizin Berlin, Department of Endocrinology and Metabolic Diseases, Charitéplatz 1, 10117 Berlin, Germany

[2]Berlin Institute of Health (BIH), Anna-Louisa-Karsch-Straße 2, 10178 Berlin, Germany

[3]DZHK (German Centre for Cardiovascular Research), partner site Berlin, Center for Cardiovascular Research (CCR), Berlin, Germany

[4]Department of Microbiology & Immunology, University of California San Francisco, 513 Parnassus Avenue, San Francisco, CA 94143, USA

[5]Gladstone Institutes, 1650 Owens Street, San Francisco, CA 94158, USA

[6]Center for Molecular Toxicology and Carcinogenesis, Department of Veterinary and Biomedical Sciences, The Pennsylvania State University, University Park, PA 16802, USA

[7]Department of Pathology, University of California San Francisco, 513 Parnassus Avenue, San Francisco, CA 94143, USA

[8]Department of Laboratory Medicine, University of California San Francisco, San Francisco, CA 94107, USA

[9]Department of Epidemiology & Biostatistics, Institute for Human Genetics, and Institute for Computational Health Sciences, University of California San Francisco, CA 94158, USA

[10]Chan Zuckerberg Biohub, San Francisco, CA 94158, USA

[*]Correspondence to: Joachim Spranger, Professor/Clinic Director, Department of Endocrinology and Metabolism, Charité-Universitätsmedizin Berlin, Charitéplatz 1, 10117 Berlin, Germany, joachim.spranger@charite.de, office: +49 (30) 450-514251, fax: +49 (30) 450-514950, Peter J. Turnbaugh, Associate Professor, Department of Microbiology & Immunology, 513 Parnassus Avenue HSW 1529, San Francisco, CA 94143-0552, USA, Peter.Turnbaugh@ucsf.edu, office: (415) 502-3237, fax: (415) 476-6185.

[&,+]These authors contributed equally

Author contributions

Manuscript preparation with input from all authors: JEB, RJvS, JS, and PJT. Human cohort design and execution RJvS, KM, and JS. Microbiome transplantation experiment design and execution: JEB, RJvS, PS, QYA, SD, MF, JAT, JS, and PJT. 16S rRNA gene sequencing and analysis: JEB, RJvS, and PS. Metagenomic sequencing and analysis: JEB, SL, RJvS, and KSP. Metabolomic quantification and analysis: JC, JEB, SLC, and ADP. *C. difficile in vitro* and gnotobiotic experiments: JEB, JAT, and PJT. Histological scoring: S-YL. *C. difficile* testing: JEB, DI, SM. Statistical analysis and data presentation: JEB, RJvS, SL, KSP, and PJT. Supervision and funding: RJvS, ADP, KSP, KM, JS, and PJT.

Competing interests

PJT is on the scientific advisory boards for Kaleido, Pendulum, Seres, and SNIPRbiome; there is no direct overlap between the current study and these consulting duties. All other authors have no relevant declarations.

Abstract

Diet is a major factor that shapes the gut microbiome[1], but the consequences of diet-induced microbiome shifts for host pathophysiology remain poorly understood. We conducted a randomized human intervention study using very-low calorie diets (VLCD). While metabolic health was improved, severe calorie restriction led to decreased bacterial abundance and restructuring of the gut microbiome. Transplantation of post-diet microbiotas to mice decreased body weight and adiposity relative to pre-diet microbiota recipients. Weight loss was associated with impaired nutrient absorption and an enrichment of *Clostridioides difficile*, which was consistent with a decrease in bile acids and sufficient to replicate metabolic phenotypes in mice in a toxin-dependent manner. These results emphasize the importance of diet-microbiome interactions in modulating host energy balance and the need to understand the role of diet in the interplay between pathogenic and beneficial symbionts.

VLCDs involve extreme calorie restriction (≤800kcal/d), typically in liquid form[2]. Gut microbial community structure and gene abundance is altered during weight loss induced by VLCDs[3,4]; however, the downstream consequences for host health and disease remain unclear. To address this knowledge gap, we performed an exploratory analysis as a component of a trial of 80 overweight/obese post-menopausal women randomized to either a medically supervised weight loss program or to a control group instructed to remain weight stable for 16 weeks[5] (Extended Data Fig. 1a). The weight loss program included 8 weeks of VLCD (800 kcal/d), 4 weeks of a conventional low-calorie diet (CONVD), and 4 weeks of weight maintenance (MAINT, Extended Data Fig. 1b). Both groups had similar baseline characteristics (Supplementary Table 1). The intervention group showed a weight reduction of 13.6±4.0% (mean±sd) relative to baseline corresponding to a loss of 12.54±3.9 kg after 12 weeks (Fig. 1a). Total caloric and macronutrient intake was lower during the VLCD, CONVD, and MAINT (Extended Data Fig. 1c,d). The VLCD lowered fat intake from baseline, whereas relative macronutrient intake was comparable to baseline in the CONVD and MAINT phases (Extended Data Fig. 1e and Supplementary Table 2). The intervention led to significantly decreased adiposity (Extended Data Fig. 1f) and improved glucose regulation (Extended Data Fig. 1g) after the VLCD. Glucose regulation reverted on the CONVD despite maintaining significantly lower adiposity; both phenotypes were stable in the control group.

The sustained and severe caloric restriction during the VLCD could have pronounced impacts on the gut microbiota analogous to long-term fasting[6,7] or parenteral nutrition[8]. Consistent with this hypothesis, the VLCD significantly decreased gut microbial colonization level measured both by fecal DNA content (Extended Data Fig. 2a) and 16S rRNA gene copies (Fig. 1b). Next, we performed 16S rRNA gene sequencing on 207 samples from 70 individuals selected based on sample availability (Supplementary Table 3). The number of denoised 16S rRNA amplicon sequence variants (ASVs) was significantly increased after the VLCD, returning to baseline levels during the CONVD (Fig. 1c). The VLCD also induced a marked, but reversible shift in gut microbial community structure. Quantification of pairwise microbial community dissimilarity relative to the baseline sample for each individual revealed a significant perturbation following the VLCD that reverted during subsequent diet phases (Extended Data Fig. 2b,c). Multivariate

comparison of community structure demonstrated significant effects of the VLCD compared to baseline that were robust to distance metric choice ($P<0.01$; ADONIS with Bray-Curtis dissimilarity). Reproducible microbial shifts were also apparent by visualizing the data via principal coordinates analysis (Extended Data Fig. 2d). To identify bacterial markers of the VLCD, we fit a random forest classifier of baseline versus VLCD in the intervention group as a function of genus-summarized abundances (Extended Data Fig. 2e). 10-fold cross validation revealed that the best classifier of VLCD versus baseline is based on 30 bacterial genera and provides minimal prediction error (11.94%). All 30 genera reverted to baseline levels during the CONVD. Closer inspection of the predictive genera revealed that the VLCD enriches for the growth of bacteria capable of foraging on host glycans (*Akkermansia*) at the expense of bacteria specialized for the metabolism of plant polysaccharides (*Roseburia, Ruminococcus, Eubacterium*)[9,10].

To more directly assess gut bacterial metabolic capacity, we performed metagenomic sequencing for 29 participants in the intervention group and 18 control subjects selected based on the availability of longitudinal sampling (Supplementary Table 3). Consistent with our amplicon-based data, metagenomic analysis revealed a transient perturbation to gut microbial community structure after the VLCD (Extended Data Fig. 2f–h). Metabolic reconstructions revealed 88 pathways, 100 modules, and 1,502 KEGG orthologies (KOs) that were differentially abundant between the VLCD and baseline samples (FDR $Q<0.1$, Supplementary Table 4). These differences were more modest comparing baseline and CONVD with only 8 differentially abundant KOs (Extended Data Fig. 2i). Next, we plotted VLCD-differential KEGG features in a functional hierarchy[11] (Fig. 1d). After the VLCD there were broad increases in the relative abundance of membrane transporters (phosphotransferase systems), enzymes involved in the import and metabolism of mono- and disaccharides, and the production of the short chain fatty acids (SCFAs) butyrate and acetate (Supplementary Table 4). The observed shifts in microbial community metabolic potential were reversible; KOs found to alter in abundance reverted during CONVD (Fig. 1d inset).

The VLCD had a pronounced impact on the abundance of bacterial genes involved in dietary and host glycan metabolism. Mapping reads to carbohydrate-active enzymes (CAZymes)[12], of the 310 CAZy families detected, 30 were significantly altered by the VLCD (FDR $Q<0.1$, Fig. 1e and Supplementary Table 5). VLCD led to a reduction in abundance of enzyme functions involved in processing plant-derived carbohydrates (cellulose, xyloglucans, and mannans). CAZy modules and enzyme families related to diet-ingredients (inulin lyase [GH91]) and mucosal glycans (host-derived sialic acid [CBM40]) and glycosaminoglycans such as keratan sulphate (GH111) were increased. CAZyme family abundances were mostly restored to baseline levels following CONVD with 6 families remaining differentially abundant relative to baseline (including CBM40; Supplementary Table 5). These results suggest that the VLCD induces marked changes to both the structure and metabolic activity of the human gut microbiome, promoting the expansion of bacteria capable of foraging on host glycans.

To further assess the impact of VLCD on microbial metabolism, we quantified two major end-products, SCFAs and branched chain amino acids (BCAAs), using targeted mass spectrometry (GC-MS) in a subset of participants based on sample availability (n=18

intervention, n=10 control). The VLCD significantly decreased the concentration of the BCAA leucine, with a trend towards decreased isoleucine and valine (Extended Data Fig. 2j). All three BCAAs were significantly decreased at the CONVD timepoint. Three major SCFAs produced by the gut microbiome: acetate, butyrate, and valerate were all significantly decreased on the VLCD (Fig. 1f). Thus, while the relative abundance of genes involved in SCFA biosynthesis increased on the VLCD, this was insufficient to compensate for the overall decrease in microbial colonization level (Extended Data Fig. 2k,l).

Microbiome transplantation experiments provided causal evidence that dietary perturbations to the gut microbiome contribute to host weight loss. We selected 5 donors that exhibited the most weight loss following the 3-month intervention; weight loss did not appear to follow a normal distribution and the top 5 individuals lost 55.6% more body weight than the average of the remaining cohort (Extended Data Fig. 3a). We transplanted stool samples collected pre- and post- 12 weeks of combined diet from the 5 donors into germ-free (GF) adult male C57BL/6J mice, after which the two recipient groups were maintained in separate isolators until the experimental endpoint (Extended Data Fig. 3b). 16S rRNA gene sequencing confirmed stable differences between recipient groups (Fig. 2a) that recapitulated multiple differences in the taxonomic composition and metabolic capacity of pre- versus post-diet humans (Extended Data Fig. 3c,d). 58 ASVs were differentially abundant between pre- and post-diet colonized mice (Extended Data Fig. 3c, Supplementary Table 6). Inferred gene abundance[13] revealed 392 KOs significantly different between pre- and post-diet colonized mice (>2-fold difference, FDR Q<0.1, LMM; Supplementary Table 7). KEGG pathway enrichment demonstrated altered functional capacity in central pathways of carbon, fatty acid, and amino acid metabolism (Extended Data Fig. 3d).

Microbiome transplantation was sufficient to induce multiple phenotypes found in human subjects during weight loss. Within 2 days post colonization, the post-diet recipients lost 12.4±5.2% (mean±sd), significantly more than the pre-diet or GF controls (Fig. 2b). This difference was maintained to 21 days post-colonization. Body fat was also significantly impacted by the post-diet gut microbiome (Fig. 2c), ameliorating the increase in adiposity typically found after colonization[14]. Colonization with pre-diet gut microbiomes had a significant impact on glucose tolerance compared to GF mice (Fig. 2d), whereas the post-diet microbial community showed an intermediate metabolic phenotype. There were no significant differences in caloric intake across the three groups (Fig. 2e); however, the caloric density of the stool was significantly higher in the post-diet as compared to the pre-diet recipients (Fig. 2f). Replication experiments with newly prepared pools of 12-week diet samples (Extended Data Fig. 4a–c), 8-week diet samples (Extended Data Fig. 4d–g), and 12-week diet samples from the 4 individuals who were closest to the median weight loss (Extended Data Fig. 4h–j) reproduced features of the initial experiment, indicating that the phenotypic consequences of diet-induced shifts in the gut microbiome are robust and not necessarily restricted to severe weight loss. Thus, the post-diet human gut microbiome contributes to weight loss in part by decreasing the efficiency of dietary energy harvest; however, microbiome-induced changes to host energy expenditure and/or resting metabolic rate remain to be explored[15].

Closer inspection of sequencing data from the initial transplantation experiment revealed the post-diet microbiota was enriched with the enteric pathogen *C. difficile* (Fig. 3a, Extended Data Fig. 3c). The most differentially abundant gene family (Extended Data Table 7) between the two recipient groups represents *C. difficile* A/B toxins (K11063, FDR $Q<0.05$, LMM), which we confirmed independently through qPCR of the *tcdB* gene (Fig. 3a). The observed difference in *C. difficile* abundance appears to represent an altered ability of the gut microbiome to restrict growth, not a difference in initial exposure, since *C. difficile* and *tcdB* were detectable at similar abundances in both recipient groups at baseline but was maintained at abundances orders of magnitude lower in pre-diet recipients (Fig. 3a). Endpoint samples from mice in both groups tested positive for toxins TcdA/TcdB and *C. difficile* by PCR and culture; however, only animals in the post-diet group had detectable levels of toxin as measured by ELISA (Extended Data Fig. 3e). Toxin was not consistently detected in our subsequent experiments (Extended Data Fig. 4k,l), potentially contributing to variation in host metabolic phenotypes.

Given the high degree of between-strain variability observed in *C. difficile*-host interactions[16], we isolated and sequenced *C. difficile* JBZPo1 from the cecum of a post-diet recipient mouse (Extended Data Fig. 5a) and used metagenomic sequencing to confirm the correct strain was isolated (see Methods). Additional molecular typing of this strain revealed that it encoded the Clostridial toxins TcdA and TcdB, but not the binary toxin associated with hypervirulent *C. difficile*[16] (Extended Data Fig. 5b,c). Multilocus sequence typing and phylogenetic analysis (Extended Data Fig. 5d) indicated that JBZPo1 likely belongs to the sequence type 2, ribotype 014–20 clade of classical non-hypervirulent *C. difficile* which is among the most commonly isolated groups in Europe[17].

To test if *C. difficile* is sufficient to replicate weight loss and metabolic phenotypes, individually housed GF C57BL/6J mice were colonized with a post-VLCD human specimen, or the same sample with the addition of *C. difficile* JBZPo1 spores (Extended Data Fig. 6a). The human-VLCD donor sample was sufficient to induce weight loss (maximum loss 6.3±2.3% mean±sd at day 1); however, the addition of the *C. difficile* spores led to increased and sustained weight loss over the duration of the experiment (maximal loss 9.4±2.3% at day 4; Fig. 3b) without causing dehydration (Extended Data Fig. 6b). Food and water consumption were not significantly different (Fig. 3c,d). *C. difficile* significantly improved glucose tolerance (Fig. 3e). While no differences in adiposity were detected at baseline, the *C. difficile*-colonized mice had significantly increased final adiposity relative to controls (Extended Data Fig. 6c). Despite the clear measurable presence of *C. difficile* and its toxins (Extended Data Fig. 6d,e) and absence in humanized controls, there were no signs of abnormal posture, behavior, or stool consistency. Gross examination of proximal colon histology did not reveal typical markers of *C. difficile*-associated colitis including hemorrhage, edema, and mucosal separation (Fig. 3f); however, blinded pathologist scoring revealed minor neutrophil infiltration with reactive changes associated with *C. difficile* colonization (Extended Data Fig. 6f).

Next, we sought to test if diet-induced shifts in the gut microbiome influence colonization resistance to *C. difficile* and thus host physiology. We colonized mice with fecal samples from the reference donor at each of the diet phases and inoculated with JBZPo1 spores

(Extended Data Fig. 7a). In both VLCD and CONVD phases, significantly higher weight loss was observed (4.6% and 6.6% respectively, Extended Data Fig. 7b). *C. difficile* colonization was similar across groups and time; however there was significantly more TcdB detected during CONVD at 2 days post-colonization suggesting that diet-microbiota interactions may affect both the outgrowth and expression of *C. difficile* virulence traits (Extended Data Fig. 7c,d).

To establish if the effects of *C. difficile* on weight and metabolism are mediated by the major virulence factors TcdA and TcdB, we obtained a toxin-deficient mutant of *C. difficile* 630[18] and replicated the experiment in GF and humanized mice (Extended Data Fig. 8a). Weight loss was induced in a toxin-dependent manner irrespective of colonization background (P_{toxin}=1e-15, LMM, Fig. 3g), despite comparable food intake (Fig. 3h). Colonization with the TcdA/B$^+$ strain led to a minor but significant decrease in water intake (Fig. 3i), without any detectable signs of dehydration (Extended Data Fig. 8b), and significantly decreased body fat (Fig. 3j). *C. difficile* was more abundant in mono-colonized mice with comparable toxin levels to humanized mice (Extended Data Fig. 8c,d). In this *C. difficile* strain, originally isolated from severe pseudomembranous colitis[19], more severe histological markers of colitis were observed (Fig. 3k, Extended Data Fig. 8e), emphasizing the utility of isolating relevant strains from the cohorts analyzed in this study.

We next sought to determine the relevance of these observations to our diet cohort and the original top 5 weight losers. While all participants were otherwise asymptomatic, screening of the top 5 losers revealed that all donors appeared to carry *C. difficile* at some point during the intervention on the basis of toxin ELISA, culture, and/or qPCR (Fig. 4a). To understand how this may be representative of the complete cohort, we turned to our metagenomic data which revealed the presence of *C. difficile* at low abundances with a ranked species abundance of 297 [52–613] (median [range]). *C. difficile* abundance varied between diet intervention participants with a significant increase in abundance observed during VLCD in the intervention group (P=0.025, Fig. 4b).

Given the previously established role of bile acids in modulating growth and germination of *C. difficile*[20,21], we quantified bile acid concentrations in donors with complete longitudinal fecal collections during the first 3 diet phases (Supplementary Table 8). Total bile acid pools were significantly decreased in response to VLCD and CONVD (Fig. 4c). We also detected a significant decrease in the *C. difficile* inhibitory bile acids deoxycholic acid (DCA) and lithocholic acid (LCA) in response to diet (Fig. 4d)[21], consistent with our colonization resistance experiment (Extended Data Fig. 7e). Decreased bile acids likely reflect a combination of less gallbladder emptying of primary bile acids due to decreased fat consumption[22] (Extended Data Fig. 1c), an overall decrease in bacterial colonization (Fig. 1b), and shifts in the abundance of bile acid metabolizing Clostridia (Extended Data Fig. 2e,h). The metabolite changes observed across the overall cohort were also reflected in the 5 donors used for our original microbiome transplantation experiment (Extended Data Fig. 9a–c).

There are multiple limitations of this work. Our clinical trial was performed at a single research site resulting in a limited sampling of geographical and ethnic backgrounds.

We only analyzed a single VLCD preparation; more work is needed to assess the generalizability of these findings to alternative formulations, including the potential impact of food matrix and preparation method[23]. *C. difficile* colonization across the full cohort was based on metagenomics. Attempts to detect toxin-positive *C. difficile* carriage by a commercial testing platform (Cepheid Xpert) were negative, potentially due to the assay design and the weak diagnostic value of detecting asymptomatic carriage[24] and/or the prolonged storage of these samples at the time of testing. Estimates of asymptomatic carriage of *C. difficile* range widely from 0–90% of individuals surveyed[25] as a function of age, exposure to health care settings, and methodology with a recent meta-analysis demonstrating a rate of 8.1% on inpatient admission[26]. Finally, our microbiome results were exploratory outcomes of this intervention study[5]; the clinical relevance of the association between *C. difficile* and weight loss outcomes requires additional human studies specifically correlating asymptomatic carriage and metabolic outcomes.

Despite these limitations, our work clearly demonstrates that severe calorie restriction leads to significant, but reversible, shifts in the human gut microbiome. Mice which received microbiome transplantations of post-diet communities replicated human phenotypes including decreased weight and adiposity, driven in part by an inability to restrict the growth of *C. difficile*. We propose a working model through which diet and *C. difficile* conspire to shape host energy balance (Extended Data Fig. 9d). More broadly, this study emphasizes the utility of coupling well-controlled clinical interventions with humanized mice, enabling the mechanistic dissection of complex relationships between the host, microbiome, and enteric pathogens.

Methods

MMS (MUSCLE METABOLISM STUDY) HUMAN COHORT

Recruitment.—Between March 2012 and July 2015, we randomized 80 overweight/obese post-menopausal women to either undergo a medically supervised weight loss and lifestyle intervention program (details below) or to remain weight stable over a period of 16 weeks, respectively. This outpatient study was conducted in our experimental and clinical research center (ECRC, Charité Campus Berlin-Buch) and participants were recruited via newspaper ads or via the endocrinological outpatient clinic. The last volunteers finished the study in September 2017, when the study ended due to completion. We used a stratified randomization scheme based on 3 BMI (body mass index: weight [kg] / height [m]^2) strata at baseline. Recruiting study nurses and physicians were blinded for the allocation sequence until inclusion of the volunteer. The allocation sequence was made via a random computer-generated list by the study PI (KM). Participants were recruited and allocated to the interventions via study physicians. The study was registered at www.clinicaltrials.gov under NCT01105143. The study was approved by the Ethik-Kommission der Charité-Universitätsmedizin Berlin. The study protocol is included as Supplementary Table 9. Informed consent was obtained from each study volunteer prior to study participation. The following conditions were used as exclusion criteria: weight loss of more than 5kg in the last 2 months, severe chronic diseases including cancer within the last 5 years, severe heart disease, severe impairment of hepatic or renal function, severe anaemia or

disturbed coagulation, eating disorders or any other psychiatric condition that would interact with the trial intervention, malabsorption, acute or chronic infections, severe hypertension, myopathy, food allergies, any other uncontrolled endocrine disorder, changes of smoking habits, diets or medication that strongly affects energy homeostasis within the last 3 months prior to study. The post-menopause status was ensured via medical history (cessation of the monthly period) and follicle stimulating hormone (FSH) screens if the status was unclear. The microbiome analysis was included in the study as a secondary outcome measurement to determine the effects of weight loss and negative energy balance on microbiome taxonomic and gene abundances. As such, the study was not designed to be powered for these specific microbiome analyses. The study protocol was amended to include the microbiome analysis and approved before recruitment. No additional documentation or consent was required for inclusion of participants in the microbiome component of the study.

Intervention.—After baseline phenotyping, volunteers belonging to the intervention group were placed on an 800 kcal/d liquid diet (Optifast, *Nestlé*) accompanied by weekly group meetings and weight loss counselling for 2 months. Thereafter, the diet was switched to a low calorie (individual daily caloric goals derived from baseline resting metabolic rate over 24 h) diet with 50–55% of total kcals derived from carbohydrates, 15–20% from protein and ~30% from fat according to a food pyramid (as recommended by the German Nutrition Society, DGE) and volunteers in the intervention group only were additionally instructed to take at least 10,000 steps per day. After 4 weeks (month 3), the weight loss intervention was completed and phenotyping was repeated. Subsequently, volunteers were instructed to maintain their weight by changing daily caloric intake goals to calories from the initial metabolic rate plus 500 kcal. Adjustments of individual intake goals were made according to body weight to achieve weight stabilization for another 4 weeks. After this weight stabilization phase, initial phenotyping was repeated.

Volunteers of the control group were instructed to keep their weight stable during the whole first 4 months which was ensured during monthly visits and nutritional counselling geared toward weight stabilization (resting metabolic rate plus 500 kcal). One volunteer (P15) was included in the study but decided to quit short before randomization which is why no baseline anthropometrics are reported. However, since this volunteer provided baseline stool samples, we chose to include this sample in the microbiome sequencing analysis as a baseline control sample.

Stool samples were collected during each phenotyping visit and additionally after 8 weeks on the liquid diet in the intervention group (Extended Data Fig. 1b). For this, volunteers were provided a stool collection kit and instructed to store collected stool samples in the freezer at −20˚C until transportation in a cooled container to our research unit. All samples were subsequently stored at −80˚C. Dietary information was assessed by dietary records at every phenotyping timepoint. Volunteers were instructed to note down every food item that was consumed throughout the four days prior to the phenotyping including the exact weight or an equivalent estimation (e.g. a teaspoon or a cup etc.). Nutrient content was estimated using Prodi v6.2 Expert. The Souci-Fachmann-Kraut-Database 2005 and the German Federal Nutrition Key (Bundeslebensmittelschlüssel) Version 3.01 were used as nutrient databases. However, even these databases do not provide nutrient data for every

kind of food item, which is why in some cases it was necessary to select a similar food instead of the actual food named in the dietary record. Therefore, one investigator performed all analyses to ensure the best possible standardization.

DNA Extraction and Sequencing.—DNA was extracted from 207 human fecal samples from 75 individuals (39 intervention and 36 control) using the QIAamp DNA Fast Stool Mini Kit (Qiagen, USA) according to the manufacturer's protocol. 16S rRNA gene PCR was carried out as before using Golay-barcoded 515F/806R primers[27] according to the methods of the Earth Microbiome Project (earthmicrobiome.org). Amplicons were quantified with PicoGreen (Quant-It dsDNA; Life Technologies) and pooled at equimolar concentrations for sequencing on an Illumina MiSeq (250×150, V3 reagents) with 10% PhiX after size selection and gel purification (QIAquick Gel Extraction Kit Qiagen). Metagenomic sequencing was performed in 161 stool samples derived from a subgroup of the study cohort (29 intervention, 18 controls; n=2–4 samples/individual). Individuals were selected based on the most complete set of phenotypic data, without taking into account inter-group differences in host or microbial phenotypes. DNA extraction, library preparation and sequencing was carried out by Eurofins Genomics, Germany using the NEBNext® Ultra™ DNA Library Prep Kit for Illumina according to the manufacturer's instructions. Metagenomic sequencing was performed on the Illumina HiSeq 2500 platform (2×125) and 4 samples per lane.

16S rRNA gene sequencing analysis.—Reads were demultiplexed using QIIME v1.9.1 (split_libraries_fastq.py) before denoising and processing with DADA2 v1.1.5[28] under MRO v3.2.5. Taxonomy was assigned using the DADA2 implementation of the RDP classifier[29] using the DADA2 formatted training sets for SILVA123 (benjjneb.github.io/dada2/assign.html). A phylogenetic tree was constructed using MUSCLE v3.8.31 and MacQIIME v1.9.1 (make_phylogeny.py) using the FastTree algorithm with midpoint rooting. Samples with less than 5,000 reads were filtered out of the datasets. Diversity metrics were generated using Vegan v2.4–3 and Phyloseq v1.20.0 with principal coordinate analysis (PCoA) carried out with Ape v4.1. Principal component analysis (prcomp; PCA) was carried out on centered log2-ratio (CLR) normalized genus abundances calculated as $A_{clr}=[\log_2(A_1/g_a), \log_2(A_2/g_a),\ldots \log_2(A_n/g_a),]$, where A is a vector of read counts with a prior of 0.5 added and g_a is the geometric mean of all values of A. Cross sectional analysis of significant features was carried out using ALDEx2 v1.8.0[30,31] using 256 simulations and Benjamini-Hochberg corrected Wilcoxon *Q*-values (paired where appropriate). For plotting purposes, $\log_2$(fold change) was considered as the difference in median CLR-normalized abundance. Random Forest analysis was carried out using randomForest v4.6.12. A Benjamini-Hochberg false discovery rate of 0.1 was used as the cutoff for statistical significance unless otherwise noted.

Metagenomic analysis.—Raw Illumina reads underwent standard quality control with fastq-mcf and host read removal by mapping to the human genome (GRCh38) with Bowtie2[32]. For functional quantification, filtered reads were mapped to the KEGG Orthology database[33] using RAPSearch2[34] and length-normalized read counts were tallied for each KO, with the exclusion of reads mapping to metazoan versions of KOs. A

subsequent adjustment for average genome size was done with MicrobeCensus[35]. Statistical testing was performed via the limma package in R, using voom normalized expression values with quality weights and the formula ~Group*Time wherein the fixed effects were treatment group (diet, control), diet phase (baseline, VLCD, CONVD, maintenance), and their interaction[36]. The differential abundance of KOs was further summarized at the module and pathway levels using mROAST[37]. Counts of CAZy family abundance were determined by DIAMOND[38] against the CAZy database. FDR corrected paired t-tests of log2 counts per million abundances were used to determine modules altered by VLCD. To normalize abundance of the abundance of butanoyl-CoA:acetoacetate CoA-transferase subunits, their abundance was determined using the reads per kilobase per genome equivalent (RPKG) mapping to the gene family (K01034) derived above and multiplying by the estimated genome equivalents per gram determined from qPCR (using 4.2 16S rRNA copies/genome to convert from 16S rRNA copies to genome equivalents). Microbial taxonomy abundances derived from shotgun sequencing were determined using Kaiju[39]. Quantification of *C. difficile* was carried out using Kraken2[40] against the Genome Taxonomy Database[41] version 89 providing equivalent results to Kaiju-determined differences in *C. difficile* abundance as a function of diet phase.

qPCR of human samples.—Quantitative PCR (qPCR) was performed on 216/290 samples that were available from the 16S rRNA gene sequencing cohort. qPCR of total 16S rRNA gene copies was carried out in triplicate 10 μL reactions with 200 nM 340F/514R primers using a BioRad CFX384 thermocycler with SYBRSelect for CFX Master Mix (Life Technologies) according to the manufacturer's instructions and an annealing temperature of 60 °C. Absolute quantifications were determined based against a standard curve of purified 8F/1542R amplified *E. coli* MG1655 DNA[42]. Reactions were performed in triplicate and mean values were taken for further downstream analyses. Absolute bacterial abundance was derived by adjustments for dilutions during DNA extraction, normalization, and PCR reaction preparation dividing by the total fecal mass used for DNA extraction in grams.

Bile acid quantification.—Human fecal samples were thawed at 4 °C and 25 mg was added to 1 mL of pre-cooled (−20 °C) methanol (containing 0.5 μM deuterated internal standards). Samples were homogenized followed by 3 cycles of freeze-thaw in liquid nitrogen. Samples were centrifuged (4 °C, 15 min, max speed) and 200 μL of the supernatant was transferred to autosampler vials for LC-MS/MS analysis. Fecal bile acids were quantified using an ACQUITY ultraperformance liquid-chromatography (UPLC) system coupled with a Xevo TQ-S triplequadrupole mass spectrometer (Waters, Milford, MA) equipped with an electrospray ionization (ESI) source operating in negative ionization mode as described[43]. SIR (m/z), MRM transitions, and retention time were developed by running individual bile acid standards. A standard curve was plotted for each individual bile acid for quantitation purposes.

SCFA and BCAA quantification.—SCFAs and BCAAs were quantified with an Agilent 7890A gas chromatograph coupled with an Agilent 5975 mass spectrometer (Agilent Technologies Santa Clara, CA) using a propyl esterification method as previously described[44,45]. Approximately 25 mg fresh human fecal samples were mixed with 1 mL of

0.005 M NaOH (containing 10 μg/mL internal standard caproic acid-6,6,6-d3), homogenized thoroughly with 1.0 mm diameter zirconia/silica beads (BioSpec, Bartlesville, OK) and centrifuged (13,200g, 4 °C, 20 min). 500 μL of supernatant was collected and mixed with an aliquot of 500 μL of 1-propanol/pyridine (v/v=3/2), then 100 μL of propyl chloroformate was added subsequently following a brief vortex for 1 minute. Samples were incubated at 60 °C for 1 hour. The derivatized samples were extracted with a two-step hexane extraction as described[45]. 300 μL of hexane was added to samples, following centrifuge (2 000g, 4 °C, 5 min) and 300 μL upper layer was transferred to an autosampler vial. Another 200 μL of hexane was added to samples and the additional 200 μL upper layer was transferred and combined with the first extraction. A total 500 μL volume of extracts were obtained for GC-MS analysis. A standard curve was drafted for each analyte to quantify biological concentration in human fecal samples.

ANIMAL EXPERIMENTS

Mice and housing.—All experiments with the exception of the median 4 weight losers (Extended Data Fig. 4h–j), were conducted at UCSF and approved by the University of California, San Francisco Institutional Animal Care and Use Committee with the support of the UCSF Gnotobiotic Core Facility. GF C57BL/6J mice aged 10–15 weeks were used for transplantation experiments. Mice were bred in-house in a sterile breeding isolator (Class Biologically Clean, USA) and transferred to an experimental isolator one week prior to experimental procedures. In all experiments, mice were fed a standard autoclaved chow diet *ad libitum* (Lab Diet 5021) with free access to water at room temperature of 24±1°C, room humidity from 30–70%, and a 12/12-h light/dark cycle (7:00 a.m.–7:00 p.m.). Baseline sterility was determined using aerobic and anaerobic culture on multiple rich media and quantitative dual-dye probe qPCR targeting the V6 region of 16S rRNA gene. Mice were singly housed with environmental enrichment in duplex cages in all experiments but the pilot transplantation experiment (Fig. 2) and median 4 weight losers (Extended Data Fig. 4h–j). The total mice per cage in these experiments ranged from (2–4) with total mice per group ranging from 3–13 as identified in Extended Data Figs. 3b, 4, 6a, 7a, and 8a.

The median 4 weight losers experiment was conducted at the Center for Cardiovascular Research at the Charité in Berlin, Germany. The experiments were performed in accordance with the terms of the German Animal Protection Law, as well as according to international animal welfare legislation and institutional ethical guidelines of the Charité Berlin, Germany, and were approved by the Landesamt für Gesundheit und Soziales (Approval number G 0085/17, LAGeSo Berlin, Germany). GF C57BL/6J mice aged 10–18 weeks were used for transplantation experiments. Mice were bred in-house in a sterile breeding isolator (North Kent Plastic, Great Britain) and transferred to an experimental isolator one week prior to experimental procedures. Mice were fed a standard autoclaved chow diet *ad libitum* with free access to water at room temperature of 24 ± 1 °C and a 12/12-h light/dark cycle (7:00 a.m.–7:00 p.m.). Baseline sterility was determined using aerobic and anaerobic culture on multiple rich media. Mice were housed in 2–4 per cage. Where multiple pre-colonization weight measurements were available for animal experiments, weight loss was normalized to their average. Mice were allocated among treatment groups balancing age and baseline weight where possible. Blinding of treatment groups was not performed.

Colonization.—Samples from multiple individuals were pooled normalizing 16S rRNA gene copies/g feces, as identified via qPCR as above, across individuals. Each fecal sample was thawed and prepared in an anaerobic chamber. A total of 1 g of fecal matter was removed and diluted with 10 ml of sterile 0.9% saline with added cysteine (0.05% w/v). Each diluted sample was then vortexed for 1 min and centrifuged at 5,000 rpm for 1 min or passed through a 100 μM mesh strainer. The resulting preparation was externally sterilized and transferred into gnotobiotic isolators wherein 200 μL was administered by oral gavage. Where spores were co-administered, they were inoculated at 1e4 spores/200μL gavage. Spores were prepared by plating a lawn of *C. difficile* on BHIS media and incubating for 7 days at 37 °C under anaerobic conditions. Plates were then washed in PBS and the resulting solution was refrigerated overnight in aerobic conditions. The preparation was then washed 3x in PBS and heated to 70 °C for 20 minutes to remove any surviving vegetative cells. Spores were enumerated under anaerobic conditions on *C. difficile* selective agar (BD) and visualized using phase contrast microscopy to verify purity of spores.

Metabolic Profiling.—Oral glucose tolerance tests were performed by fasting mice for 6 hours, and then administering 2 mg/kg glucose by oral gavage. Blood glucose was measured at 0, 15, 30, 60, and 120 minutes after gavage using a OneTouch Ultra 2 (LifeScan, USA). Body fat was measured by either EchoMRI for whole-body fat composition, or dissection and weighing of the epididymal fat pad. Food and water intake were measured for individual mice longitudinally at each timepoint collecting body mass (in experiments using singly housed cages), or for the cage in aggregate (for experiments involving cohousing). In the pilot fecal transplantation experiment (Fig. 2), food consumption was measured at days 7–10, 10–14, 14–18 and 18–20. For this experiment, food intake per mouse per day was calculated as follows: [total food intake per cage]/[mice per cage]/[days of food consumption]. Caloric intake was determined by converting to kcal using the value 4.62 kcal/g gross energy for Lab Diet 5021. To measure fecal energy content, fecal pellets were collected from individual mice and lyophilized for 24 h prior to determination of energy content via bomb calorimetry. After completion of the drying process, the dried masses of the pellets were recorded. Gross energy content was measured using an isoperibol oxygen bomb calorimeter with a semimicro oxygen bomb (Models 6200 and 1109, respectively, from Parr Instrument Co). The calorimeter energy equivalent factor was determined using benzoic acid standards. Sample dropouts occurred due to misfire and were accounted for by using linear mixed models for statistical analysis.

Histology.—Proximal colon samples were transferred to cassettes and preserved overnight in 10% neutral buffered formalin before transfer to ethanol and storage at 4˚C. Samples were subsequently embedded in paraffin, sectioned (4μM), and H&E stained. Slides were blindly scored according to the methodology of Erben *et al.*[46].

16S rRNA Gene Sequencing and Analysis.—DNA samples were extracted from 48 mouse fecal samples via bead beating for 4 min (Min-Beadbeater-24, BioSpec), using Lysing Matrix E (MPBio) using the lysis buffer of a Wizard SV 96 Genome DNA kit (Promega) with subsequent DNA isolation according to the manufacturer's protocol. Amplification was conducted by combining 2 μL of DNA with 25 μL of AmpliTaq Gold 360

Master Mix (Life Technologies), 5 μL of primers (2 μM each GoLay-barcoded 515/806R), and 18 μL H_2O. Amplification was as follows: 10 min 95˚C, 30x (30s 95˚C, 30s 50˚C, 30s 72˚C), and 7 min 72˚C. Data was processed as described above for the MMS human cohort.

Time-course analysis of the mouse experiment was carried out using ZIBR v0.1[47] including random effects to account for repeated sampling across time using the Benjamin-Hochberg corrected joint *Q*-value, unless 0 values comprised >90% or <10 % for the given feature, in which case only the logistic or beta component was considered, respectively. For plotting purposes, $\log_2$(fold change) was considered as the difference in median CLR-normalized abundance. Gene content based on 16S rRNA gene sequencing data was inferred using PICRUSt v1.0.0 based on closed reference OTU assignments to the Greengenes May 2013 release using QIIME v1.9.1. These were compared via linear mixed effect model as before with mouse as a random effect with FDR $Q<0.1$ considered as statistically significant. KEGG Pathway enrichment was carried out using clusterProfiler v3.4.1. Engraftment of ASVs from the pooled human sample (Fig. 2a) was quantified at 36% and 52% for pre- and post-diet recipient groups, respectively, and 66% and 83% at the genus level in line with previous reports[48,49].

***C. difficile* testing, quantification, and isolation.—**Direct culture was carried out using BBL *Clostridium difficile* selective agar (CDSA; Becton, Dickson and Company). Samples were thawed in an anaerobic chamber (Coy Lab Products) and ~ 10 mg of feces was directly applied to agar using a four-quadrant streak method. Plates were incubated for 72 h at 37˚C in 5% CO_2, 10% H_2, and 85% N_2. Plates were then removed from anaerobic conditions and imaged under normal and long-wave UV light. Positive specimens were determined by the presence of at least one colony fitting the *C. difficile* morphology: yellow, ground-glass, slightly filamentous edges with fluorescence under long-wave UV light. ELISA was carried out using a commercial kit according to the manufacturer's instructions (TGC-E001–1, tgcBiomics) detecting both TcdA and TcdB toxins with detection limits of 0.5 and 1 ng/mL, respectively. Endpoint PCR for *tcdA* and *tcdB* was carried out using a multiplexed assay according the protocol of Persson, Torpdahl, and Olsen[50] excluding the 16S rRNA gene primer set of the 5-plex on previously sequenced DNA extracted with the modified Promega approach above. *C. difficile* and *tcdB* were quantified via qPCR using the following oligonucleotides[51]: 5-GCAAGTTGAGCGATTTACTTCGGT-3($P_{CD\text{-}forward}$), 5-GTACTGGCTCACCTTTGATATTYAAGAG-3($P_{CD\text{-}reverse}$), 5-[6FAM]TGCCTCTCAAATATATTATCCCGTATTAG[BHQ1]-3($P_{CD\text{-}probe}$), and 5-TACAAACAGGTGTATTTAGTACAGAAGATGGA-3($P_{tcdB\text{-}forward}$), 5-CACCTATTTGATTTAGMCCTTTAAAAGC-3($P_{tcdB\text{-}reverse}$), 5-[HEX]TTTKCCAGTAAAATCAATTGCTTC[BHQ1]-3($P_{tcdB\text{-}probe}$).

qPCR was conducted using iTaq Universal Probes Supermix (BioRad) according to manufacturer's instructions with an annealing temperature of 56.6 °C with a CFX384 thermocycler (BioRad). The limit of detection was estimated to be 1e3 genome equivalents/g on the basis of extraction of a dilution series of *C. difficile* JBZPo1. Remaining aliquots of 61human fecal samples were assayed via the Cepheid Xpert C.diff-Epi assay version 2 at the UCSF Clinical Microbiology lab. All assayed samples tested negative for Toxin B, Binary Toxin, and TcdC, including those which had previously been assayed positive

via ELISA, qPCR, and culture. Sample remnants were then subjected to an enrichment culture algorithm by incubating for 72h at 37˚C in CCMB-TAL (Anaerobe systems) with ELISA performed for TcdA/B as above on 48h and 72h supernatants. qPCR with the above primers/probes was carried out after 72h with DNA extracted using the ZymoBIOMICS 96 MagBead DNA kit according to the manufacturer's protocol. After 48h, CCMB-TAL was subcultured onto CDSA and representative colonies were subcultured and their 16S rRNA sequence determined (GeneWiz Sequencing). A total of 18 samples were presumptively positive on the basis of culture morphologies consistent with C. difficile; however, after sequencing these were primarily determined to represent *Clostridium innocuum*. One sample contained a genuine *C. difficile* isolate (MMSP50 CONVD timepoint) and no isolate could be obtained from the previously ELISA-positive sample (MMSP30 CONVD timepoint). ELISA and qPCR of enriched cultures confirmed this result with no detectable toxin A/B or amplicon respectively.

***C. difficile* JBZPo1 and genetic characterization.—**Metagenomic sequencing of fecal DNA from a subset of recipient mice (Fig. 2a, Supplementary Table 3), was performed. Libraries were prepared using the Nextera XT protocol according to the manufacturer's instructions and sequenced by Illumina NovaSeq with paired end 140×140 reads obtaining 0.56 – 16.10 Gbp per sample. To generate a draft assembly of the potential causative *C. difficile* strain, a cross-assembly was created from all samples within the post-diet recipient mice (Megahit[52]), and then these assemblies were used to generate metagenome assembled genomes (MAGs) using composition and abundance across samples[53]. A total of 204 MAGs were assigned taxonomy using MetaWrap[54] and a single *C. difficile* genome was recovered estimated at 96.66% completion with 0.43% contamination on the basis of single copy marker genes[55]. A sequencing library was prepared from gDNA of the JBZPo1 isolate using the Nextera XT protocol according to the manufacturer's instructions (Illumina) and sequenced using paired end 251×251 reads (V3 MiSeq chemistry) with a total of 2,780,073 reads after demultiplexing. Reads were filtered using Trimmomatic[56] and assembled using SPAdes 3.11.1[57]. The resulting assembly was submitted to NCBI PGAP for annotation. Comparison of JBZPo1 to the *C. difficile* MAG was conducted using pyani[58] finding a whole genome average nucleotide identity of >99.9%. This genome was placed in a phylogenetic tree using Phylophlan[59] using available *C. difficile* genomes retrieved from the PATRIC[60] with ribotypes retrieved based on literature review. The presence of *tcdA, tcdB, cdtR, cdtA,* and *cdtB* was determined based on BLAST. Multilocus sequence typing was performed with mlst (github.com/tseemann/mlst).

STATISTICAL ANALYSIS

All statistics were carried out in R version 3.4.0 or 3.6.1 using Welch's *t*-tests or Wilcoxon rank sum and signed rank tests where appropriate unless otherwise indicated. For non-microbiome related analyses, linear mixed effects models (LMMs) were performed using lmerTest[61] with multiple testing corrections via ghlt function of multcomp using Tukey's all-pair comparison method. For non-normally distributed variables, a Kruskal-Wallis test followed by Dunn's post hoc test was performed as implemented with the dunn.test package in R (version 1.3.5). Graphical representation was carried out using ggplot2 unless otherwise stated[62]. Values are presented as mean±sem unless otherwise noted. In boxplots,

the centerline represents the median with the limits representing the 1st and 3rd quartiles with whiskers extending up to 1.5x the interquartile range and outliers shown as individual points when all points have not been plotted (n<10). For analysis of weight changes in mice, weights were normalized to the average of run-in samples where available to calculate the percent change in body weight and carried forward for statistical analysis. Area under the curve was calculated as either the total area under the curve (AUC) using the trapezoid rule, or the incremental AUC (iAUC) as per the method of Brouns *et al.*[63].

DATA AVAILABILITY

16S rRNA gene and metagenomic sequencing reads have been deposited in the SRA under BioProject PRJNA412411. The genome of *C. difficile* JBZPo1 has been deposited under BioProject PRJNA503906. The following public databases were used: The Genome Taxonomy Database (), DADA2 Taxonomic Training Sets (benjjneb.github.io/dada2/assign.html), CAZy (cazy.org), and KEGG (genome.jp/kegg).

Extended Data

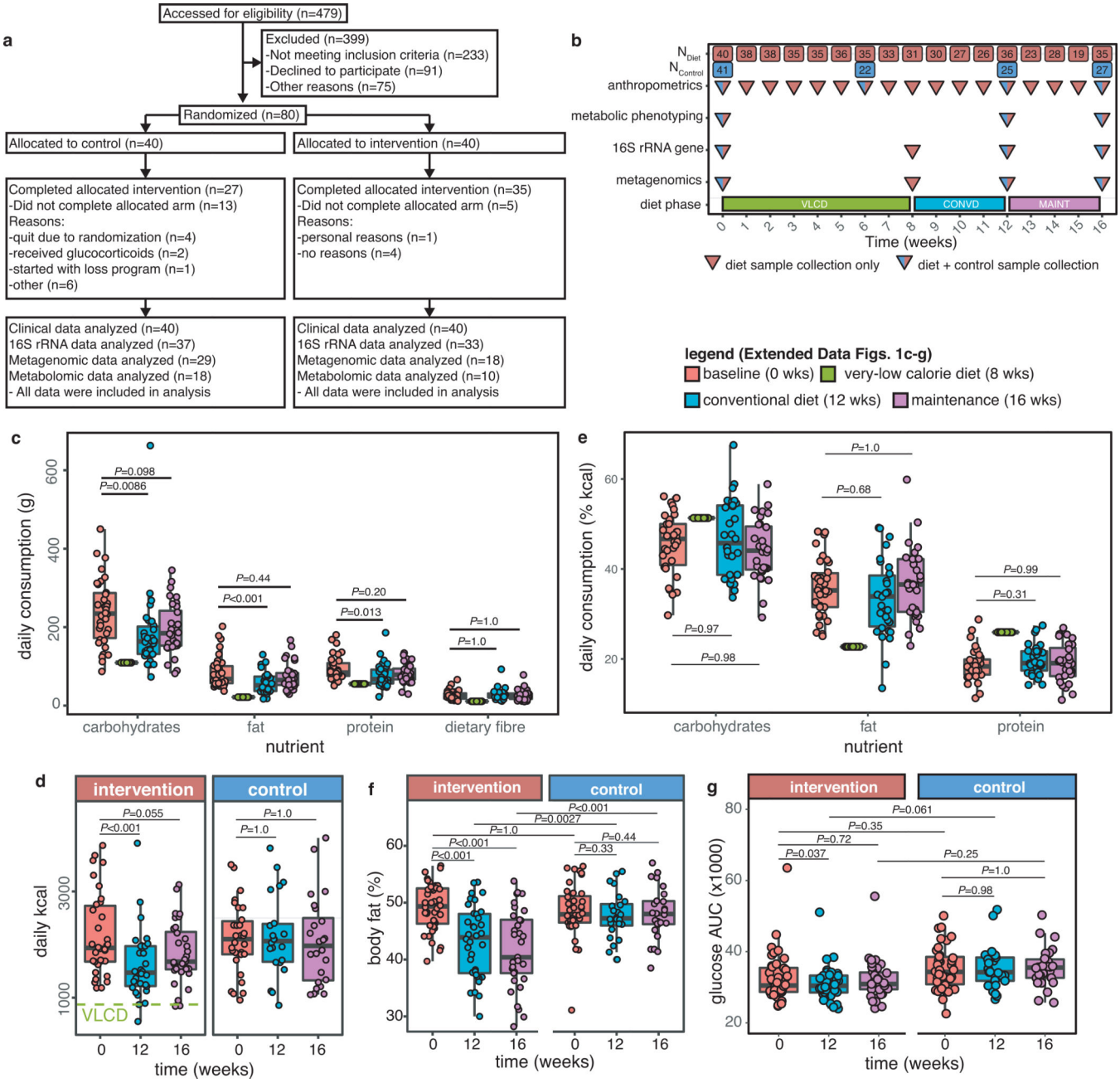

Extended Data Figure 1. MMS diet intervention study.

a, CONSORT diagram describing enrollment, allocation, and data analysis. **b,** Per timepoint group sizes and timing of data collection. Participants in the diet group underwent 2 months of a very-low calorie liquid diet followed by an additional month of a conventional low-calorie diet. During the 4th month, they were instructed to maintain weight stable. During all diet periods individuals were counseled by clinical nutritionists. Timepoints with data collection are shown for both diet and control participants. Daily consumption of macronutrients measured by **c,** mass and **e,** percentage of daily energy intake in diet

group ($n_{baseline}$=34, n_{VLCD}=34, n_{CONVD}=30, n_{MAINT}=32 participants). **d,** Total daily caloric intake during diet phases ($n_{intervention}$ as in panels c and e, control group $n_{baseline}$=30, n_{CONVD}=22, n_{MAINT}=24 participants) **f,** Decreases in relative body fat are observed in the intervention group ($n_{baseline}$=40, n_{CONVD}=36, n_{MAINT}=33 participants) relative to the control group ($n_{baseline}$=40, n_{CONVD}=24, n_{MAINT}=26 participants). **g,** Diet leads to improvement in glucose tolerance as measured by oral glucose tolerance test within and between diet ($n_{baseline}$=40, n_{CONVD}=36, n_{MAINT}=35 participants) and control ($n_{baseline}$=40, n_{CONVD}=25, n_{MAINT}=26 participants) groups. Statistical testing performed by LMM with Tukey's two-sided all-pair comparison. In boxplots, the median is represented by the center line with the box representing the 1st and 3rd quartiles, whiskers extend 1.5x the interquartile range with outliers individually plotted.

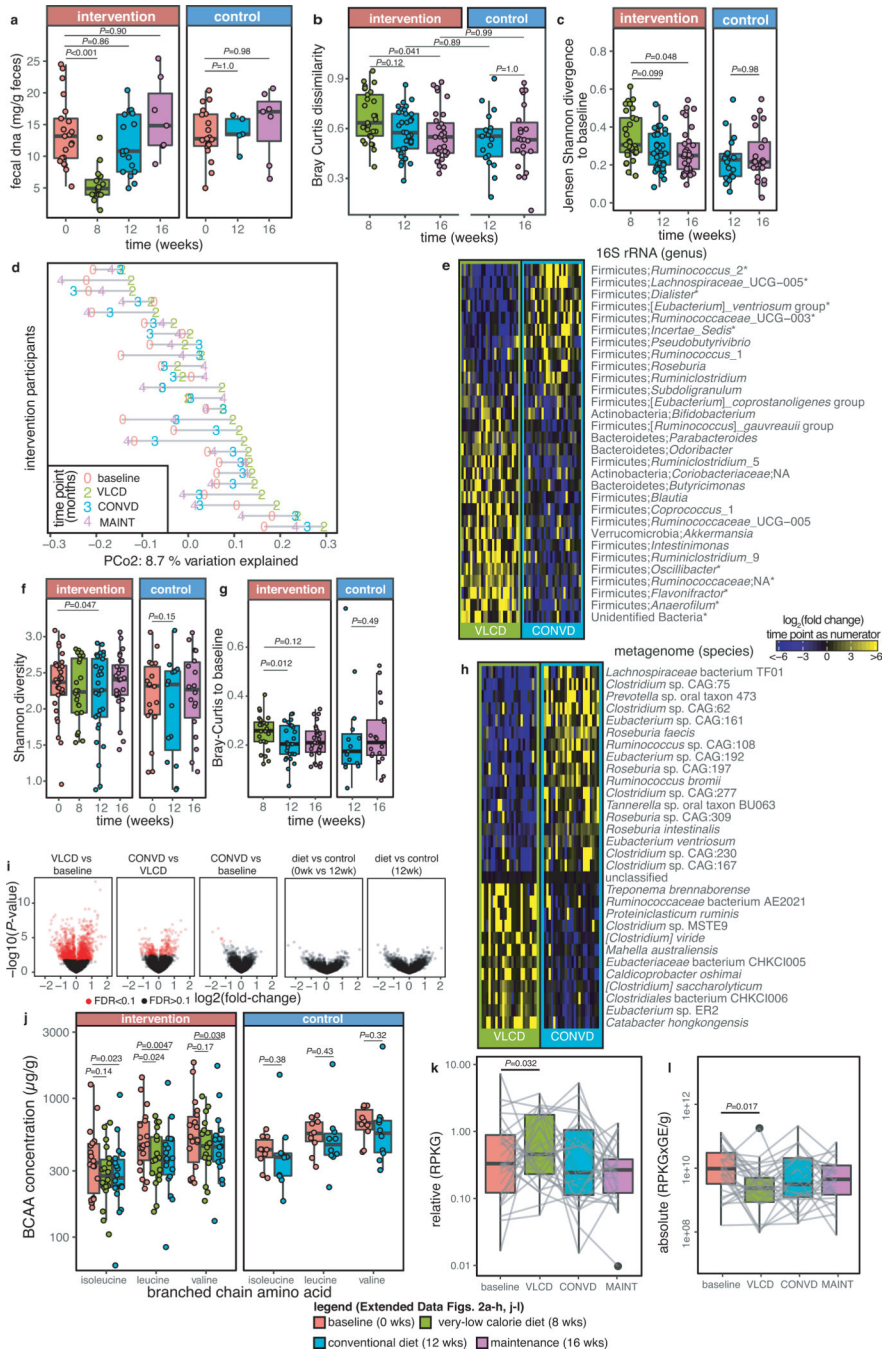

Extended Data Figure 2. Reproducible and reversible shifts are observed in the gut microbiota as a result of caloric restriction in both 16S rRNA amplicon and shotgun metagenomic sequencing data.

a, Concentration of fecal DNA reveals decreased microbiota abundances in response to VLCD contrasting within diet ($n_{baseline}$=21, n_{VLCD}=16, n_{CONVD}=17, n_{MAINT}=7 participants) and between control ($n_{baseline}$=19, n_{CONVD}=5, n_{MAINT}=7 participants) groups. Microbiotas determined by 16S rRNA gene sequencing revert to a state more closely resembling baseline samples after VLCD (n=19–33/group/timepoint as listed in Supplementary Table 3) by both **b,** Bray-Curtis Dissimilarity and **c,** Jensen Shannon

divergence (also $P<0.001$ $R^2=0.031$ ADONIS with Participant ID as stratum). **d,** Reproducible shifts in community membership are observed across individuals on the second principal coordinate in response to diet followed by reversion during conventional diet and maintenance (Unweighted UniFrac). Each series of connected points represents a single individual in the study with the number representing the timepoint of the study in months. **e,** Genera whose abundances are altered by VLCD demonstrate rapid reversion during the conventional diet (30 most important genera by GINI coefficient displayed, Random Forest, *FDR $Q<0.1$ ALDEx2). **f,** Shannon diversity is significantly decreased after conventional diet ($P=0.047$, n=29, mean difference = 0.149 [0.002 – 0.296 95%CI], paired Welch's two-sided *t*-test). **g,** Microbiotas revert to a state more closely resembling baseline samples after VLCD, as measured through species-level metagenomic assignments ($P=0.012$, n=15–29/group/timepoint as listed in Supplementary Table 3, two-sided Wilcoxon signed rank test). **h,** Metagenomic species whose abundances are altered by VLCD demonstrate rapid reversion during the conventional diet and maintenance phases (30 most important genera by GINI coefficient displayed. **i,** Volcano plot of differentially abundant KEGG orthologies (KOs) by contrast in metagenome data. VLCD demonstrates the largest effect size with apparent reversion when contrasted against CONVD (conventional diet). Effects of CONVD compared to baseline, and cross-group comparisons yield minimal significant results. Statistical analysis was conducted with Limma. **j,** Branched chain amino acids leucine and isoleucine are significantly reduced during VLCD ($n_{intervention}=18$, $n_{control}=10$ participants/timepoint, Wilcoxon signed-rank test)**. k,** The butanoyl-CoA:acetoacetate CoA-transferase alpha subunit, an enzyme catalyzing the final step in the production of butyrate, is increased in relative abundance (RPKG reads per kilobase per genome equivalent; *FDR* $Q=0.032$ Limma; Supplementary Table 4). **l,** Normalizing relative abundance of butanoyl-CoA:acetoacetate CoA-transferase with qPCR quantification of 16S rRNA gene copies to infer the absolute number of genome equivalents (GE) in the sample demonstrates a decrease in the absolute abundance of the enzyme family ($P=0.017$, LMM with Tukey two-sided all-pair comparison). Sample size in number of participants for panels k and l are $n_{baseline}=29$, $n_{VLCD}=24$, $n_{CONVD}=29$, $n_{MAINT}=28$. In boxplots, the median is represented by the center line with the box representing the 1st and 3rd quartiles, whiskers extend 1.5x the interquartile range with outliers individually plotted.

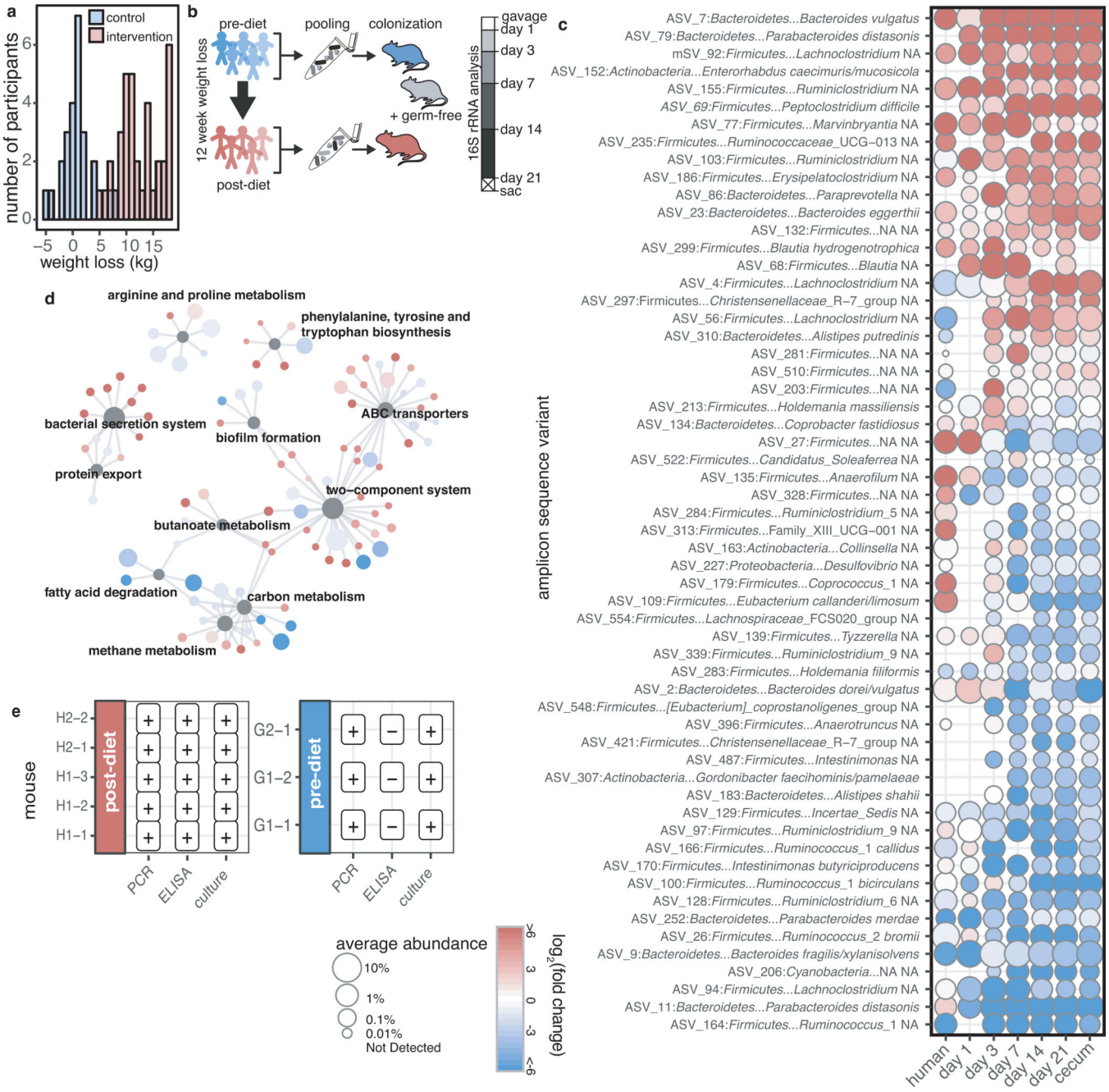

Extended Data Figure 3. Diet-dependent changes in the microbiome are maintained following transplantation to germ-free mice.

a, Distribution of weight loss in diet intervention participants identifies the 5 individuals that lost the most weight for transplantation to GF C57BL/6J mice. **b,** Experiment design and microbiota sampling times. **c,** Differential 16S rRNA amplicon sequence variant (ASV) abundances in human donors and recipient mice demonstrates 58 candidate effectors of the weight loss phenotype (ZIBR FDR Q<0.1, Supplementary Data Table 6). Note: taxonomy assigned using SILVA 123 with *Peptoclostridium difficile* synonymous for *C. difficile.* **d,** Functional differences between pre- and post-diet recipient communities by

enrichment of KEGG functional pathways based on inferred gene content from amplicon sequencing (PICRUSt, Supplementary Data Table 7). Contrasting groups predicts altered amino acid, carbohydrate, and SCFA metabolic function. Central nodes represent KEGG pathways significantly enriched by their constituent significant differentially abundant KEGG orthologies shown with fold change (color) and FDR value (size) indicated (FDR $Q<0.1$, LMM). **e,** Detection of *C. difficile* and TcdA/TcdB by endpoint PCR, ELISA, and selective and differential culture demonstrates active toxin production in post-diet mice at sacrifice.

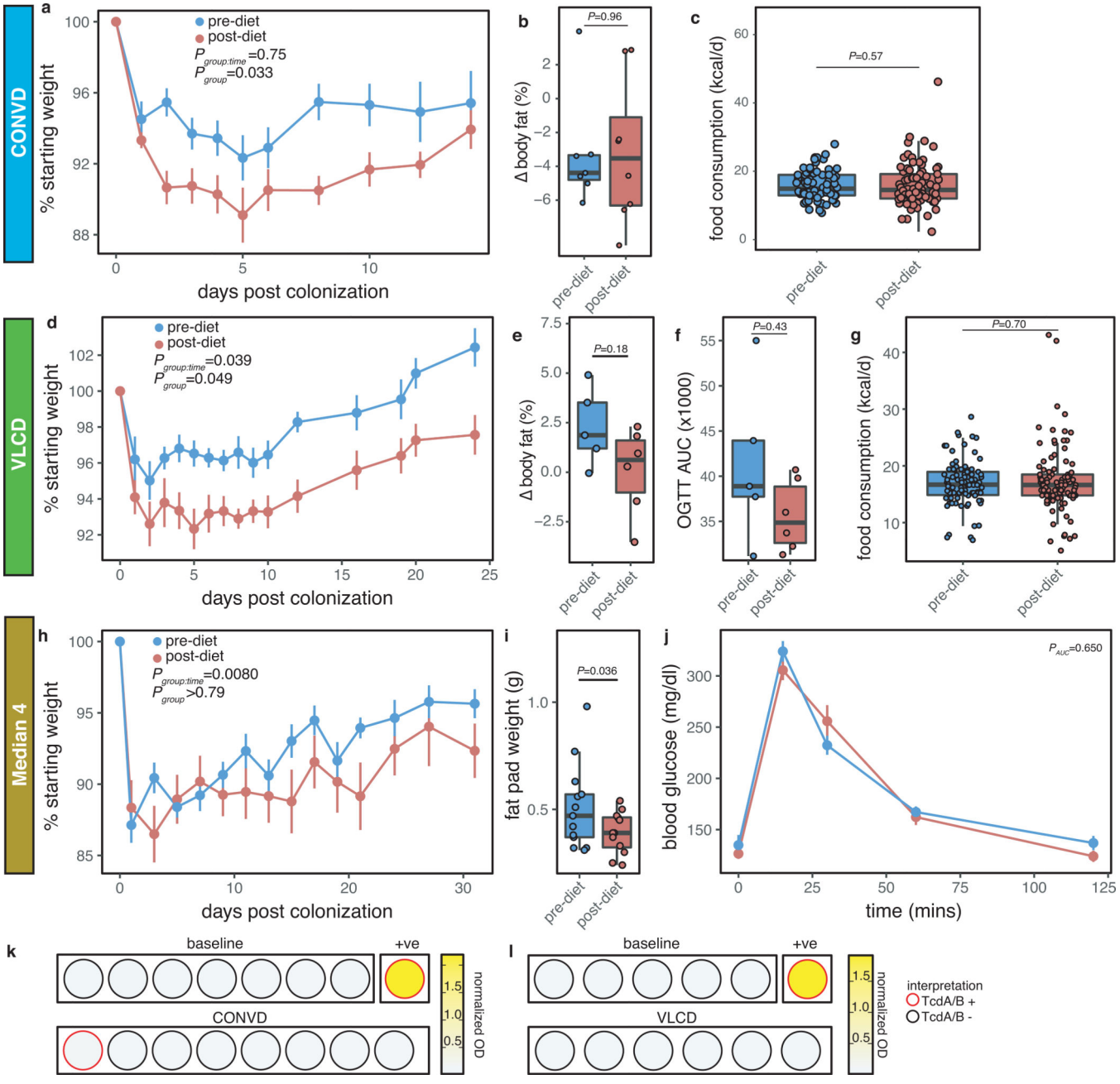

Extended Data Figure 4. Replication microbiome transplantation experiments.

a, Replication of top 5 weight losers during conventional diet demonstrates significant differences in body weight between pre- and post-diet mice (Fig. 2b) without significant differences in **b,** body fat and **c,** food consumption. *(*$n_{pre\text{-}diet}$=7, $n_{post\text{-}diet}$=8 mice, LMM). Each point in panel c represents the measurement for a single mouse at a single day. **d,** Transplantation of pooled fecal samples from top 5 weight losers during VLCD reveals significantly more weight loss in post-diet recipient mice (LMM). **e,** A trend in reduced body fat and **f,** OGTT are observed in post-diet recipient mice (P=0.18 and P=0.43 respectively, two-sided Mann-Whitney U test). $n_{pre\text{-}diet}$=5, $n_{post\text{-}diet}$=6 mice in panels d-f. **g,** Food intake is not significantly different between pre- and post-diet recipient mice over time and between groups (P=0.70, LMM $n_{\text{post-diet}}$=6, $n_{\text{pre-diet}}$=5 mice measured over 16 timepoints as identified in panel d). **h,** Transplantation of pooled fecal samples from the median 4 weight losers reveals a small but significant effect on weight gain in recipient mice (LMM, $n_{pre\text{-}diet}$=13, $n_{post\text{-}diet}$=12 mice/timepoint) with **i,** associated reduction in body fat as measured by epididymal fat pad weight (P=0.036, one-tailed Welch's t-test). **j,** No significant differences are observed in oral glucose tolerance tests in this cohort (area under the curve, P=0.650, two-sided Mann-Whitney U test). Error bars represent mean±SEM where relevant. TcdA/B ELISA demonstrates a lack of stable *C. difficile* colonization in **k,** CONVD and **l,** VLCD replication experiments (ELISA reactions shown for individual animals at days 4 and 20 post colonization respectively). Linear mixed effects models (LMM) with participant as random effect and Tukey two-sided all-pair comparison unless otherwise noted. In boxplots, the median is represented by the center line with the box representing the 1st and 3rd quartiles, whiskers extend 1.5x the interquartile range with outliers individually plotted.

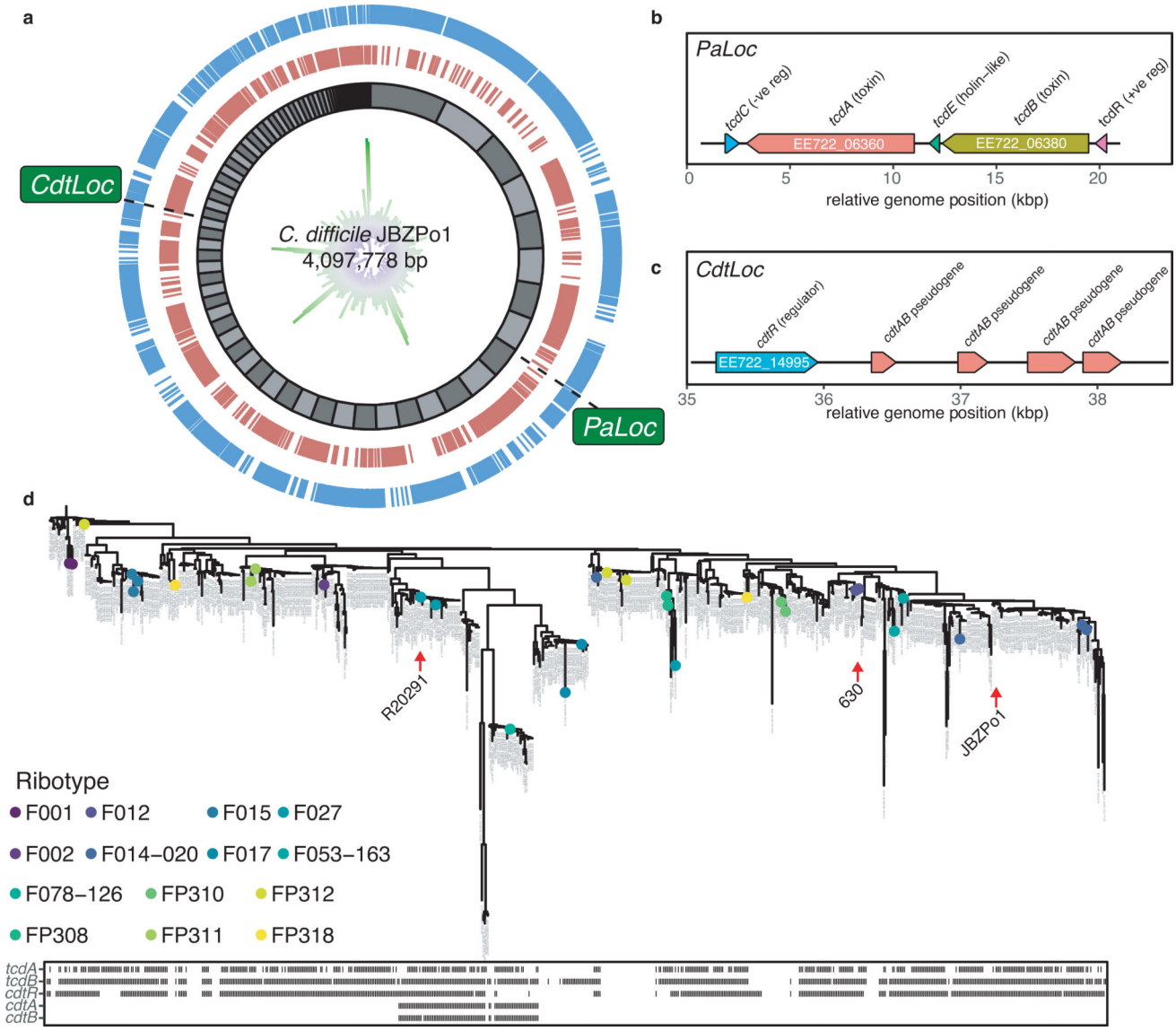

Extended Data Figure 5. Characterization of *C. difficile* JBZPo1.

a, JBZPo1 was assembled with 255-fold coverage (Illumina MiSeq 250) into 120 contigs (inner grey track, N50=87,201bp) with an average GC content of 28.6% (green-purple center track showing GC content), and 3,777 CDS (outer red and blue tracks displaying + and - strands respectively). **b,** *C. difficile* pathogenicity locus (PaLoc) encodes both toxin A (*tcdA*) and B (*tcdB*). **c,** The binary toxin (*cdt*) locus (CdtLoc) does not encode intact binary toxin. **(d)** Phylogenetic tree of 717 *C. difficile* genomes and associated virulence factor carriage places JBZPo1 flanked by Ribotype 014–20 strains and separate from the hypervirulent epidemic NAP1/B1/027 strains (ex. R20291).

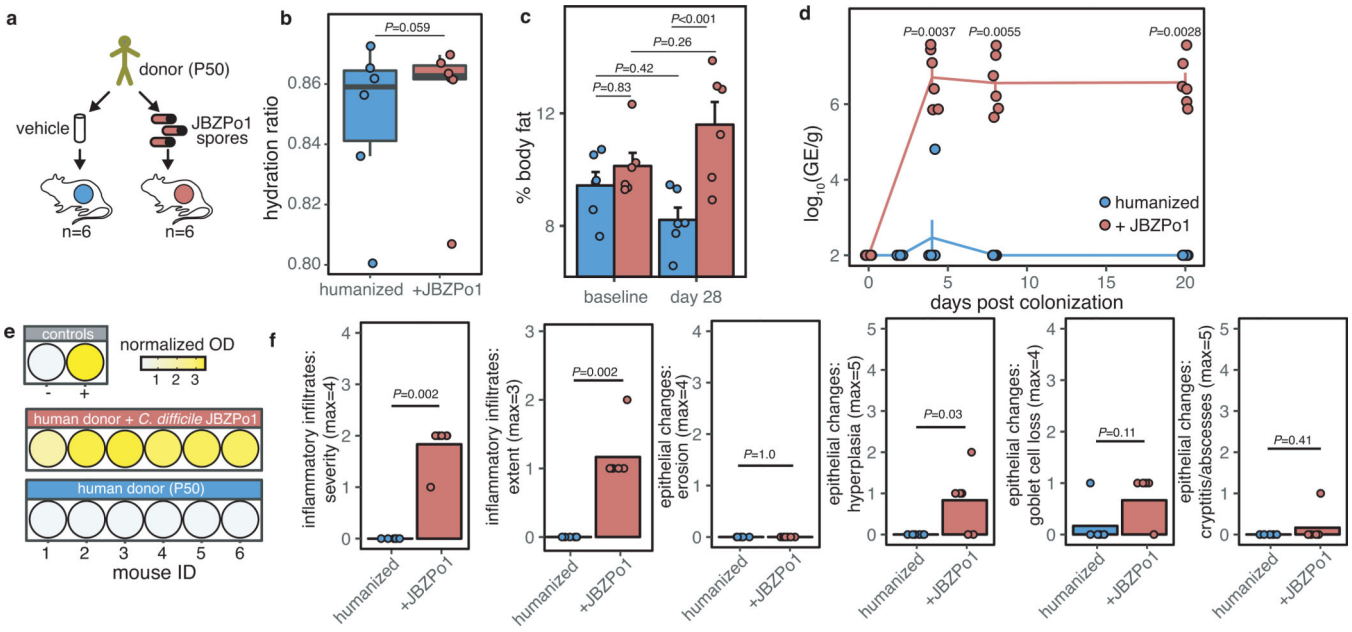

Extended Data Figure 6. Extended data relating to *C. difficile* sufficiency experiments.

a, Experimental design relating to JBZPo1 transplantation experiment (Fig. 3b). **b,** Establishment of colonization with *C. difficile* JBZPo1 does not lead to dehydration as determined by hydration ratio (hydration ratio = [total body water - free water] / lean mass; P=0.59, two-sided Mann-Whitney U test). In panel b, the median is represented by the center line with the box representing the 1st and 3rd quartiles, whiskers extend 1.5x the interquartile range with outliers individually plotted. **c,** Body composition analysis revealed a significantly difference between humanized vehicle control and *C. difficile* mice at sacrifice (P<0.001, LMM with Tukey's two-sided all-pair comparison, n=6/group) suggesting that *C. difficile* led to increased adiposity. **d,** Quantification of JBZPo1 in recipient mice (P=0.003–0.006, n=6 mice/group/timepoint except n=5 mice at 8 days in humanized control due to missing sample, two-sided Mann-Whitney U test). Error bars represent the mean±SEM. **e,** Cecal contents ELISA of recipient mice confirmed production of TcdA/TcdB in only JBZPo1 recipient mice at sacrifice. **f,** Blinded pathological analysis reveals minor neutrophil infiltration with reactive changes (two-sided Mann-Whitney U test, n=6 mice/group).

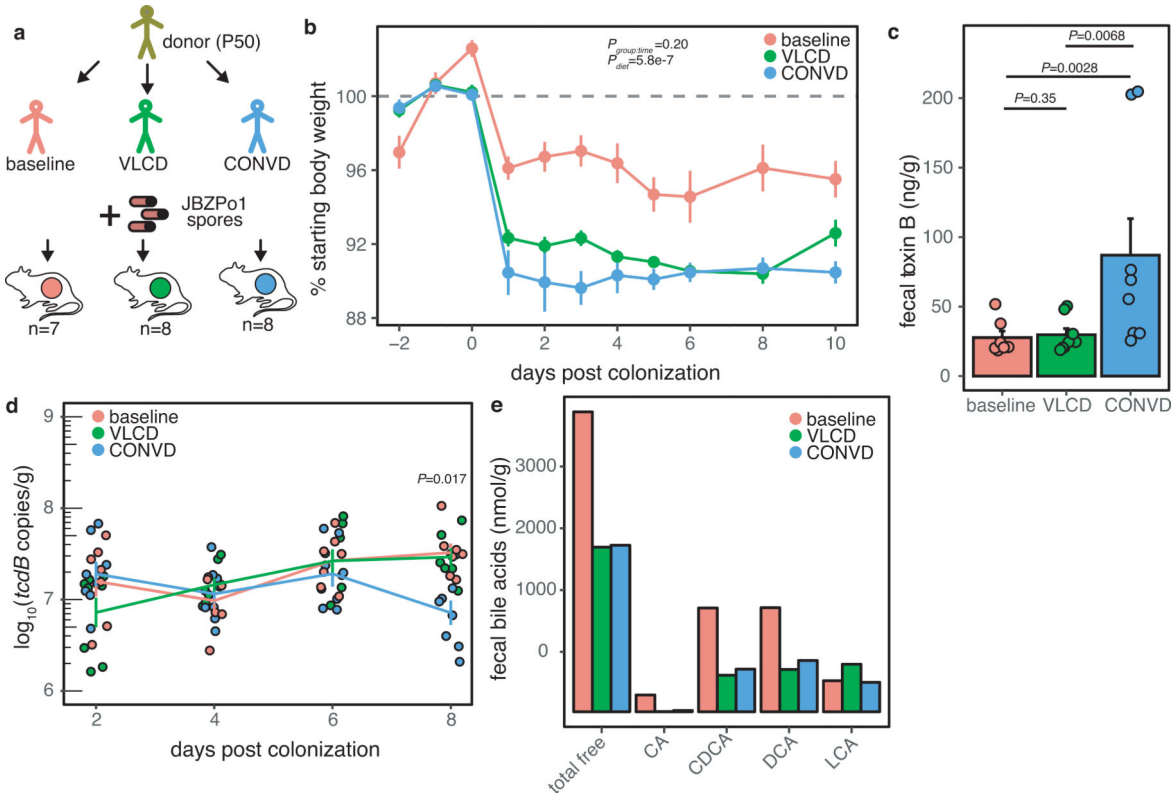

Extended Data Figure 7. Diet-induced microbiota shifts influence *C. difficile*-associated weight loss and Toxin B expression.

a, Experimental design. **b,** Weight loss over time demonstrates a significant effect of Diet (n=7–8 mice/group/day as indicated in panel a, *P*=5.9e-5, estimate= −4.6 % [−6.6 - −2.7 95%CI] [VLCD], *P*=1.5e-7, estimate= −6.6 % [−8.5 - −4.6 95%CI] [CONVD]). **c,** Higher TcdB expression is observed in CONVD-colonized mice at 2 days post colonization versus baseline (*P*=0.003, n=7–8 mice/group as indicated in panel a, Kruskal-Wallis with two-sided Dunn's Test). **d,** *C. difficile* carriage is not significantly different suggesting modulation of virulence, with the exception of 8 days post colonization in VLCD-recipient mice (P=0.017 CONVD vs baseline, n=7–8 mice/group as indicated in panel a, two-sided Mann-Whitney U test). Error bars represent the mean±sSEM in panels c and d. **e,** Concentrations of key bile acids in P50 in response to diet (n=1 participant/timepoint). Linear mixed effects models (LMM) with participant as random effect and Tukey two-sided all-pair comparison unless otherwise noted.

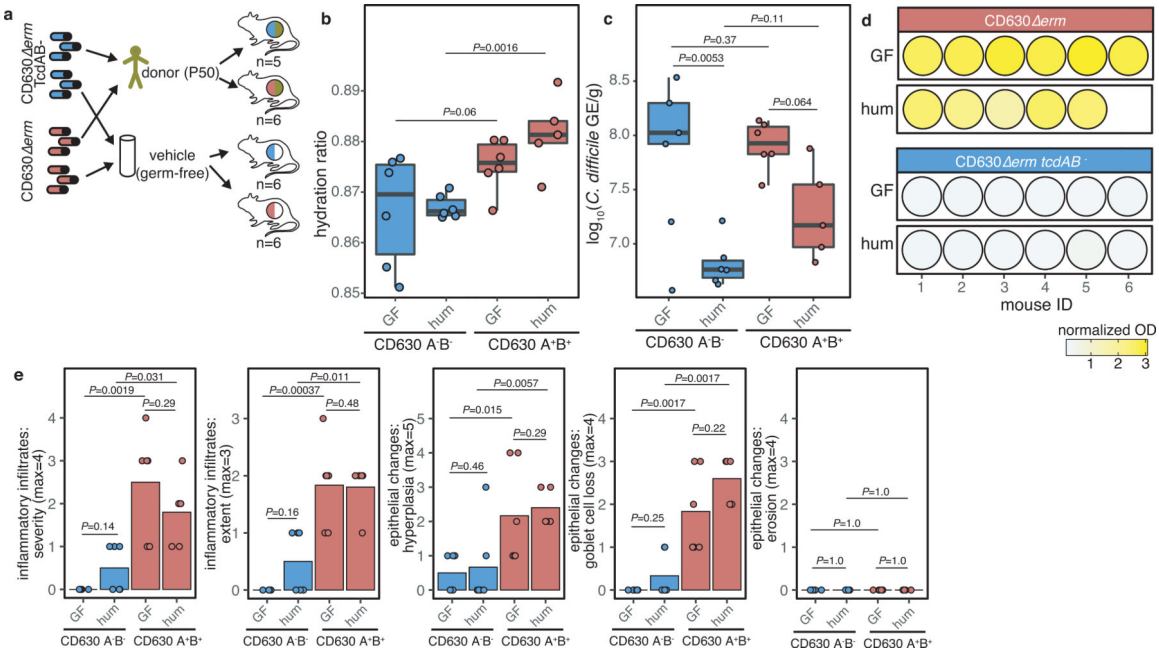

Extended Data Figure 8. Extended Data relating to necessity of Toxins A and B in metabolic phenotypes.

a, Experimental design relating to *C. difficile* 630 toxin-deficient mutant transplantation experiment (Fig. 3g). **b,** Colonization with TcdA/B$^+$ strains does not lead to dehydration in GF animals and increases hydration in humanized animals (*P*=0.06 and *P*=0.0016 respectively, Kruskal-Wallis with two-sided Dunn's Test). **c,** Cecal *C. difficile* colonization level is not significantly different between strains (*P*=0.37 and *P*=0.11 for GF and humanized respectively, Kruskal-Wallis with two-sided Dunn's Test), but is altered in mono-colonization versus humanized mice. **d,** Cecal contents ELISA confirms production of toxin in only *C. difficile* 630 Δ*erm* mutants. **e,** dense neutrophil and lymphocyte infiltration along with moderate epithelial hyperplasia and goblet cell loss due to TcdA$^+$ TcdB$^+$ *C. difficile* irrespective of colonization background (Kruskal-Wallis test with two-sided Dunn's post-hoc test). In panels b-e, n=5–6 mice/group as indicated in panel a.

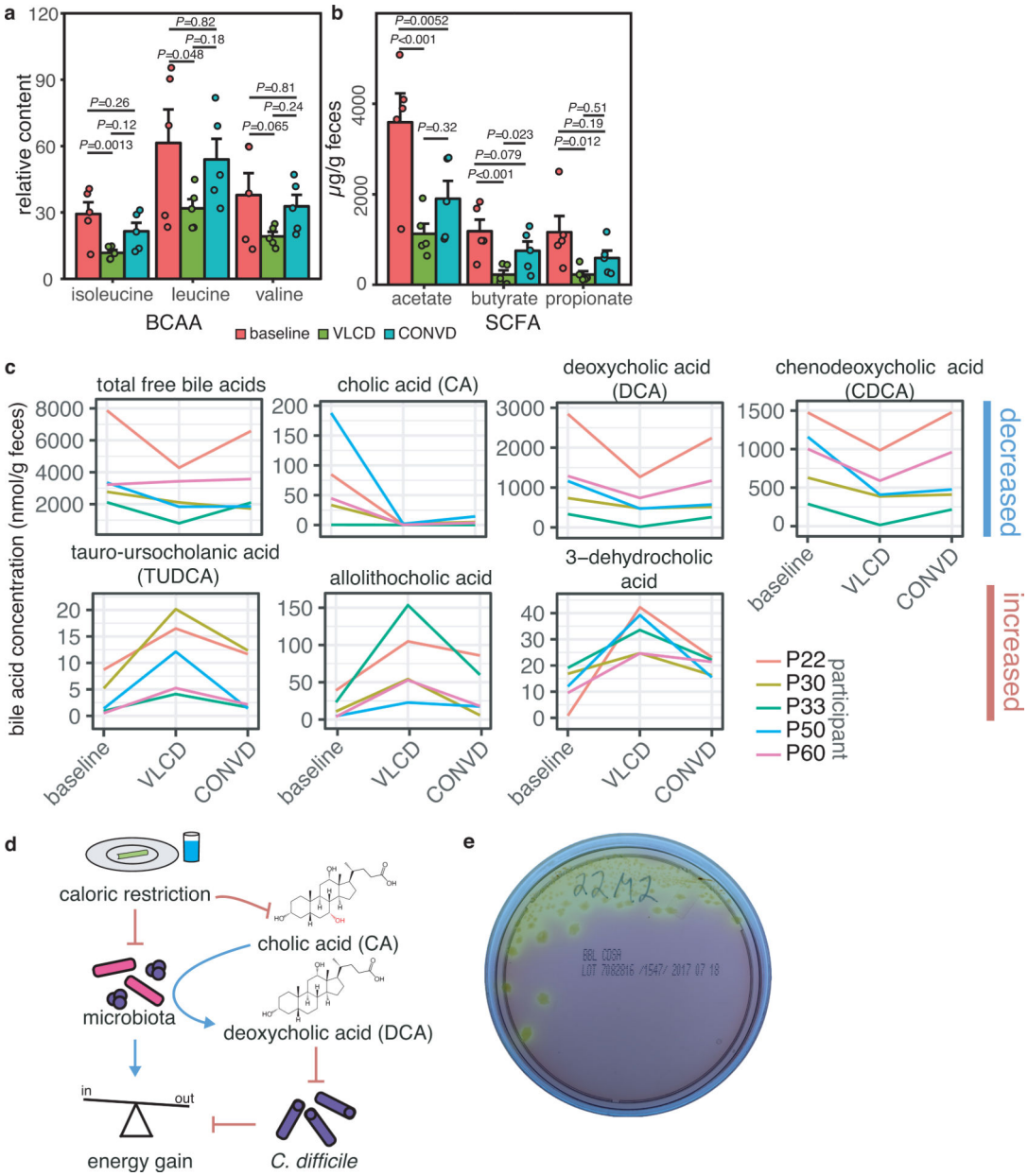

Extended Data Figure 9. Metabolomic profiling of top 5 weight losers subgroup supports A working model for the impact of caloric restriction on colonization resistance.

a, Branched chain amino acid and **b,** short-chain fatty acids are decreased during VLCD and CONVD relative to baseline in top 5 weight losers (n=5 individuals/timepoint). **c,** Significantly different bile acid levels in top 5 weight losers implicate altered bile acid profiles in permissibility to *C. difficile* (n=5 individuals/timepoint). Error bars represent mean±SEM where applicable. Statistical testing for panels a-c done via LMM with Tukey's two-sided all-pair comparison. **d,** Working model for the complex interactions between caloric restriction, the gut microbiome, and *C. difficile*. We propose that caloric restriction decreases host production of primary bile acids, including cholic acid (CA), while also lowering total gut microbial colonization, and shifting gut microbial community structure.

Together, these effects lead to the decreased production of the *C. difficile*-inhibitory deoxycholic acid (DCA) allowing for expansion of *C. difficile* which in turn disrupts host energy balance. Importantly, our data also supports *C. difficile*-independent mechanisms for weight loss due to the restructuring of the gut microbiome following caloric restriction. **e,** Representative culture plate showing presumptive *C. difficile* colonies with characteristic yellow appearance and filamentous edges.

Supplementary Material

Refer to Web version on PubMed Central for supplementary material.

Acknowledgements

We are indebted to the UCSF Gnotobiotic Core Facility, and the Lynch lab (UCSF) for technical support. Furthermore, we gratefully acknowledge Sebastian Brachs from the Spranger Lab for technical and scientific support of the animal experiments. We also thank Dr. Philip B. Smith in the Metabolomics Facility of Penn State. The Turnbaugh lab was supported by the National Institutes of Health (R01HL122593; R21CA227232; P30DK098722; 1R01AR074500; 1R01DK114034) and the Sugar, Stress, Environment, and Weight (SSEW) Center. PJT was a Chan Zuckerberg Biohub investigator and a Nadia's Gift Foundation Innovator supported, in part, by the Damon Runyon Cancer Research Foundation (DRR-42-16), the UCSF Program for Breakthrough Biomedical Research (partially funded by the Sandler Foundation), and the Searle Scholars Program. JEB was the recipient of a Natural Sciences and Engineering Research Council of Canada Postdoctoral Fellowship and received support from the National Institute of Allergy and Infectious Diseases (K99AI147165). PS was supported by the Canadian Institutes of Health Research Fellowship program. QYA was the recipient of a graduate fellowship from A*STAR (Agency for Science, Technology and Research), Singapore. Funding was also provided by the Berlin Institute of Health (JS, RJS, KM) and the German Research Foundation (DFG) to JS (CRC/TR 296 Locotact, CRG192 and CRG218) as well as the DZHK (German Centre for Cardiovascular Research) partner site Berlin (RJS, JS), DZD (German Centre for Diabetes Research) partner site Berlin (JS), and the BMBF (German Ministry of Education and Research) (KM, JS). RJS was a participant in the BIH Charité Clinician Scientist Program funded by the Charité-Universitätsmedizin Berlin and the Berlin Institute of Health. Further funding was provided by the Einstein Foundation Berlin via the Einstein Center for Regenerative Therapies (RJS). Funding support was also provided via the Gladstone Institutes and NSF grant #DMS-1850638 (KSP).

References

1. David LA et al. Diet rapidly and reproducibly alters the human gut microbiome. Nature 505, 559–563 (2014). [PubMed: 24336217]
2. Johansson K, Neovius M & Hemmingsson E Effects of anti-obesity drugs, diet, and exercise on weight-loss maintenance after a very-low-calorie diet or low-calorie diet: a systematic review and meta-analysis of randomized controlled trials. Am. J. Clin. Nutr 99, 14–23 (2014). [PubMed: 24172297]
3. Louis S, Tappu RM, Damms-Machado A, Huson DH & Bischoff SC Characterization of the Gut Microbial Community of Obese Patients Following a Weight-Loss Intervention Using Whole Metagenome Shotgun Sequencing. PLoS One 11, e0149564 (2016). [PubMed: 26919743]
4. Heinsen F-A et al. Beneficial Effects of a Dietary Weight Loss Intervention on Human Gut Microbiome Diversity and Metabolism Are Not Sustained during Weight Maintenance. Obes. Facts 9, 379–391 (2016). [PubMed: 27898428]
5. Spranger L et al. Thrifty energy phenotype predicts weight regain – results of a randomized controlled trial. Preprint at 10.1101/2021.03.25.21254300v1 (2021).
6. Kohl KD, Amaya J, Passement CA, Dearing MD & McCue MD Unique and shared responses of the gut microbiota to prolonged fasting: a comparative study across five classes of vertebrate hosts. FEMS Microbiol. Ecol 90, 883–894 (2014). [PubMed: 25319042]
7. Zarrinpar A, Chaix A, Yooseph S & Panda S Diet and feeding pattern affect the diurnal dynamics of the gut microbiome. Cell Metab. 20, 1006–1017 (2014). [PubMed: 25470548]
8. Harris JK et al. Specific microbiome changes in a mouse model of parenteral nutrition associated liver injury and intestinal inflammation. PLoS One 9, e110396 (2014). [PubMed: 25329595]

9. van Passel MW et al. The genome of *Akkermansia muciniphila,* a dedicated intestinal mucin degrader, and its use in exploring intestinal metagenomes. PLoS One 6, e16876 (2011). [PubMed: 21390229]
10. Morrison DJ & Preston T Formation of short chain fatty acids by the gut microbiota and their impact on human metabolism. Gut Microbes 7, 189–200 (2016). [PubMed: 26963409]
11. Uchiyama T, Irie M, Mori H, Kurokawa K & Yamada T FuncTree: Functional Analysis and Visualization for Large-Scale Omics Data. PLoS One 10, e0126967 (2015). [PubMed: 25974630]
12. Lombard V, Golaconda Ramulu H, Drula E, Coutinho PM & Henrissat B The carbohydrate-active enzymes database (CAZy) in 2013. Nucleic Acids Res. 42, D490–5 (2014). [PubMed: 24270786]
13. Langille MG et al. Predictive functional profiling of microbial communities using 16S rRNA marker gene sequences. Nat. Biotechnol 31, 814–821 (2013). [PubMed: 23975157]
14. Backhed F et al. The gut microbiota as an environmental factor that regulates fat storage. Proc. Natl. Acad. Sci. U. S. A 101, 15718–15723 (2004). [PubMed: 15505215]
15. Cani PD et al. Microbial regulation of organismal energy homeostasis. Nat Metab 1, 34–46 (2019). [PubMed: 32694818]
16. Hunt JJ & Ballard JD Variations in virulence and molecular biology among emerging strains of *Clostridium difficile*. Microbiol. Mol. Biol. Rev 77, 567–581 (2013). [PubMed: 24296572]
17. Bauer MP et al. *Clostridium difficile* infection in Europe: a hospital-based survey. Lancet 377, 63–73 (2011). [PubMed: 21084111]
18. Kuehne SA et al. The role of toxin A and toxin B in *Clostridium difficile* infection. Nature 467, 711–713 (2010). [PubMed: 20844489]
19. Wüst J, Sullivan NM, Hardegger U & Wilkins TD Investigation of an outbreak of antibiotic-associated colitis by various typing methods. J. Clin. Microbiol 16, 1096–1101 (1982). [PubMed: 7161375]
20. Buffie CG et al. Precision microbiome reconstitution restores bile acid mediated resistance to *Clostridium difficile*. Nature 517, 205–208 (2015). [PubMed: 25337874]
21. Sorg JA & Sonenshein AL Bile salts and glycine as cogerminants for *Clostridium difficile* spores. J. Bacteriol 190, 2505–2512 (2008). [PubMed: 18245298]
22. Festi D et al. Gallbladder motility and gallstone formation in obese patients following very low calorie diets. Use it (fat) to lose it (well). Int. J. Obes. Relat. Metab. Disord 22, 592–600 (1998). [PubMed: 9665682]
23. Carmody RN et al. Cooking shapes the structure and function of the gut microbiome. Nat. Microbiol 4, 2052–2063 (2019). [PubMed: 31570867]
24. Fang FC, Polage CR & Wilcox MH Point-Counterpoint: What Is the Optimal Approach for Detection of *Clostridium difficile* Infection? J. Clin. Microbiol 55, 670–680 (2017). [PubMed: 28077697]
25. Furuya-Kanamori L et al. Asymptomatic Clostridium difficile colonization: epidemiology and clinical implications. BMC Infect. Dis 15, 516 (2015). [PubMed: 26573915]
26. Zacharioudakis IM, Zervou FN, Pliakos EE, Ziakas PD & Mylonakis E Colonization With Toxinogenic *C. difficile* Upon Hospital Admission, and Risk of Infection: A Systematic Review and Meta-Analysis. Am. J. Gastroenterol 110, 381–390 (2015). [PubMed: 25732416]

References for Methods

27. Caporaso JG et al. Ultra-high-throughput microbial community analysis on the Illumina HiSeq and MiSeq platforms. ISME J. 6, 1621–1624 (2012). [PubMed: 22402401]
28. Callahan BJ et al. DADA2: High-resolution sample inference from Illumina amplicon data. Nat. Methods 13, 581–583 (2016). [PubMed: 27214047]
29. Wang Q, Garrity GM, Tiedje JM & Cole JR Naive Bayesian classifier for rapid assignment of rRNA sequences into the new bacterial taxonomy. Appl. Environ. Microbiol 73, 5261–5267 (2007). [PubMed: 17586664]

30. Fernandes AD, Macklaim JM, Linn TG, Reid G & Gloor GB ANOVA-like differential expression (ALDEx) analysis for mixed population RNA-Seq. PLoS One 8, e67019 (2013). [PubMed: 23843979]
31. Fernandes AD et al. Unifying the analysis of high-throughput sequencing datasets: characterizing RNA-seq, 16S rRNA gene sequencing and selective growth experiments by compositional data analysis. Microbiome 2, 15 (2014). [PubMed: 24910773]
32. Langmead B & Salzberg SL Fast gapped-read alignment with Bowtie 2. Nat. Methods 9, 357–359 (2012). [PubMed: 22388286]
33. Kanehisa M, Goto S, Sato Y, Furumichi M & Tanabe M KEGG for integration and interpretation of large-scale molecular data sets. Nucleic Acids Res. 40, D109–14 (2012). [PubMed: 22080510]
34. Zhao Y, Tang H & Ye Y RAPSearch2: a fast and memory-efficient protein similarity search tool for next-generation sequencing data. Bioinformatics 28, 125–126 (2012). [PubMed: 22039206]
35. Nayfach S & Pollard KS Average genome size estimation improves comparative metagenomics and sheds light on the functional ecology of the human microbiome. Genome Biol. 16, 51 (2015). [PubMed: 25853934]
36. Law CW, Chen Y, Shi W & Smyth GK voom: Precision weights unlock linear model analysis tools for RNA-seq read counts. Genome Biol. 15, R29 (2014). [PubMed: 24485249]
37. Wu D et al. ROAST: rotation gene set tests for complex microarray experiments. Bioinformatics 26, 2176–2182 (2010). [PubMed: 20610611]
38. Buchfink B, Xie C & Huson DH Fast and sensitive protein alignment using DIAMOND. Nat. Methods 12, 59–60 (2015). [PubMed: 25402007]
39. Menzel P, Ng KL & Krogh A Fast and sensitive taxonomic classification for metagenomics with Kaiju. Nat. Commun 7, 11257 (2016). [PubMed: 27071849]
40. Wood DE, Lu J & Langmead B Improved metagenomic analysis with Kraken 2. Genome Biol 20, 257 (2019). [PubMed: 31779668]
41. Chaumeil P-A, Mussig AJ, Hugenholtz P & Parks DH GTDB-Tk: a toolkit to classify genomes with the Genome Taxonomy Database. Bioinformatics 36, 1925–1927 (2019).
42. Edwards U, Rogall T, Blocker H, Emde M & Bottger EC Isolation and direct complete nucleotide determination of entire genes. Characterization of a gene coding for 16S ribosomal RNA. Nucleic Acids Res. 17, 7843–7853 (1989). [PubMed: 2798131]
43. Sarafian MH et al. Bile acid profiling and quantification in biofluids using ultra-performance liquid chromatography tandem mass spectrometry. Anal. Chem 87, 9662–9670 (2015). [PubMed: 26327313]
44. Cai J et al. Orthogonal Comparison of GC-MS and 1H NMR Spectroscopy for Short Chain Fatty Acid Quantitation. Anal. Chem 89, 7900–7906 (2017). [PubMed: 28650151]
45. Zheng X et al. A targeted metabolomic protocol for short-chain fatty acids and branched-chain amino acids. Metabolomics 9, 818–827 (2013). [PubMed: 23997757]
46. Erben U et al. A guide to histomorphological evaluation of intestinal inflammation in mouse models. Int. J. Clin. Exp. Pathol 7, 4557–4576 (2014). [PubMed: 25197329]
47. Chen EZ & Li H A two-part mixed-effects model for analyzing longitudinal microbiome compositional data. Bioinformatics 32, 2611–2617 (2016). [PubMed: 27187200]
48. Turnbaugh PJ et al. The effect of diet on the human gut microbiome: a metagenomic analysis in humanized gnotobiotic mice. Sci. Transl. Med 1, 6ra14 (2009).
49. Fouladi F et al. Sequence variant analysis reveals poor correlations in microbial taxonomic abundance between humans and mice after gnotobiotic transfer. ISME J. 14, 1809–1820 (2020). [PubMed: 32313261]
50. Persson S, Torpdahl M & Olsen KE New multiplex PCR method for the detection of Clostridium difficile toxin A (tcdA) and toxin B (tcdB) and the binary toxin (cdtA/cdtB) genes applied to a Danish strain collection. Clin. Microbiol. Infect 14, 1057–1064 (2008). [PubMed: 19040478]
51. Kubota H et al. Longitudinal Investigation of Carriage Rates, Counts, and Genotypes of Toxigenic *Clostridium difficile* in Early Infancy. Appl. Environ. Microbiol 82, 5806–5814 (2016). [PubMed: 27451451]

52. Li D, Liu C-M, Luo R, Sadakane K & Lam T-W MEGAHIT: an ultra-fast single-node solution for large and complex metagenomics assembly via succinct de Bruijn graph. Bioinformatics 31, 1674–1676 (2015). [PubMed: 25609793]

53. Alneberg J et al. Binning metagenomic contigs by coverage and composition. Nat. Methods 11, 1144–1146 (2014). [PubMed: 25218180]

54. Uritskiy GV, DiRuggiero J & Taylor J MetaWRAP—a flexible pipeline for genome-resolved metagenomic data analysis. Microbiome 6, 1–13 (2018). [PubMed: 29291746]

55. Parks DH, Imelfort M, Skennerton CT, Hugenholtz P & Tyson GW CheckM: assessing the quality of microbial genomes recovered from isolates, single cells, and metagenomes. Genome Res. 25, 1043–1055 (2015). [PubMed: 25977477]

56. Bolger AM, Lohse M & Usadel B Trimmomatic: a flexible trimmer for Illumina sequence data. Bioinformatics 30, 2114–2120 (2014). [PubMed: 24695404]

57. Bankevich A et al. SPAdes: a new genome assembly algorithm and its applications to single-cell sequencing. J. Comput. Biol 19, 455–477 (2012). [PubMed: 22506599]

58. Pritchard L, Glover RH, Humphris S, Elphinstone JG & Toth IK Genomics and taxonomy in diagnostics for food security: soft-rotting enterobacterial plant pathogens. Anal. Methods 8, 12–24 (2015).

59. Segata N, Börnigen D, Morgan XC & Huttenhower C PhyloPhlAn is a new method for improved phylogenetic and taxonomic placement of microbes. Nat. Commun 4, 2304 (2013). [PubMed: 23942190]

60. Wattam AR et al. Improvements to PATRIC, the all-bacterial Bioinformatics Database and Analysis Resource Center. Nucleic Acids Res. 45, D535–D542 (2017). [PubMed: 27899627]

61. Kuznetsova A, Brockhoff PB & Christensen RHB lmerTest package: tests in linear mixed effects models. J. Stat. Softw 82, 1–26 (2017).

62. Wickham H ggplot2: Elegant Graphics for Data Analysis. (Springer-Verlag New York, 2016).

63. Brouns F et al. Glycaemic index methodology. Nutr. Res. Rev 18, 145–171 (2005). [PubMed: 19079901]

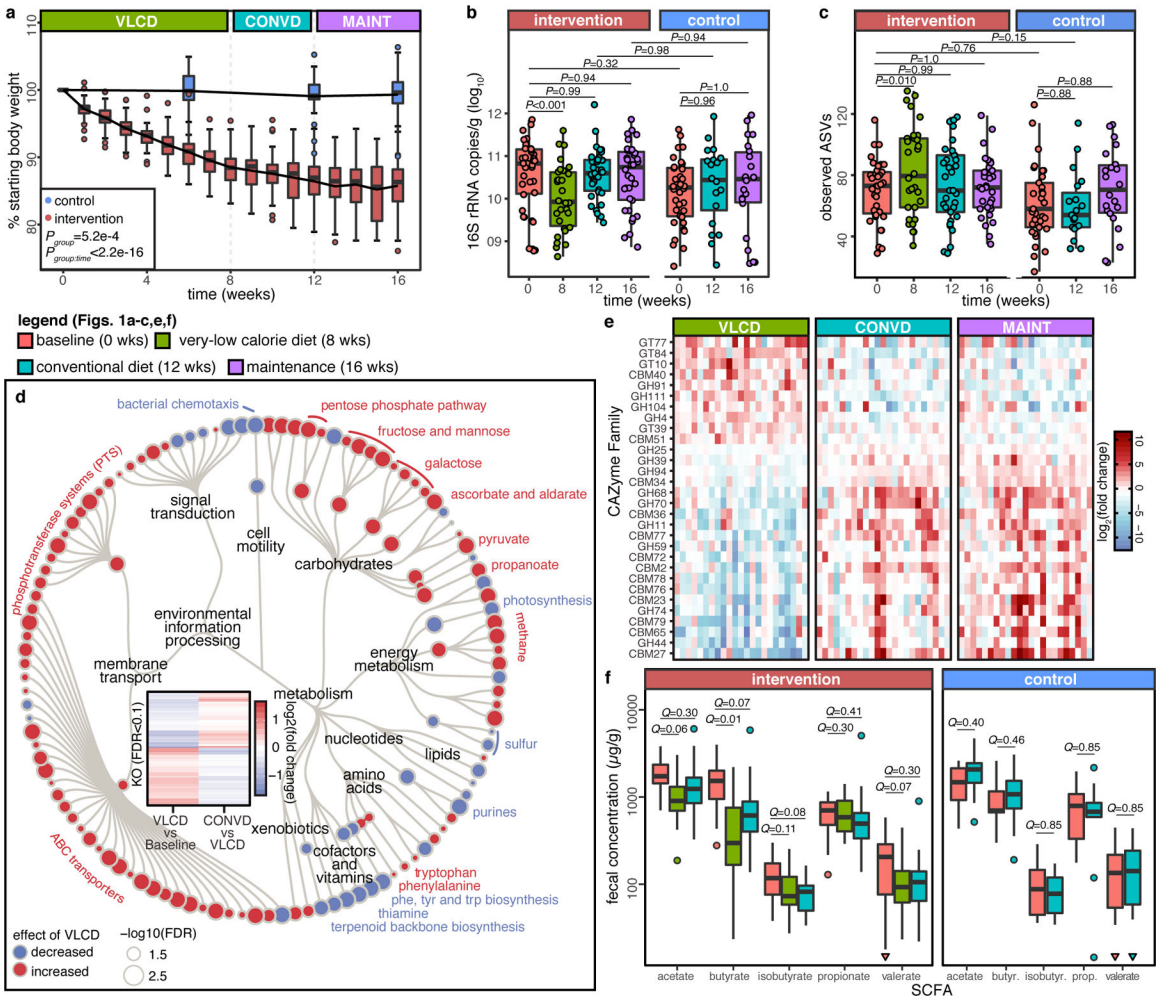

Figure 1. Very low-calorie diets alter microbiota composition and activity.

a, Diet participants lost significantly more weight over time versus controls over the combined 12-week intervention (0.84%/week [0.68–1.0 95%CI], P<2.2e-16, LMM, $n_{control}$=40, $n_{intervention}$=40 participants). **b,** The VLCD decreases overall gut microbial colonization as demonstrated by qPCR-based quantification of 16S rRNA gene copies per gram wet weight (P<0.001, $n_{\text{intervention}}$ n=39, n_{control} n=35 participants, LMM). **c,** Richness of 16S rRNA gene sequence variants (ASVs) increases following the consumption of VLCD (P=0.010, $n_{\text{intervention}}$=37, n_{control}=32 participants, negative binomial generalized LMM). **d,** Microbiome functional capacity, as measured through shotgun metagenomic sequencing, is altered by VLCD (Supplementary Table 4; FDR Q<0.1, Limma and mROAST). The tree demonstrates a functional hierarchy where inner nodes and outer tips represent pathways and modules respectively. (Inset) A heatmap of significantly different KEGG Orthologies (KOs) demonstrates their reversion when contrasted against the CONVD where minimal differences are observed relative to baseline (Extended Data Fig. 2i). **e,** Heat map of diet-induced changes to carbohydrate active enzymes (CAZymes, FDR Q<0.1 two-sided paired t-test VLCD vs baseline) demonstrates that changes revert in subsequent timepoints (Supplementary Table 5). **f,** Short-chain fatty acids acetate, butyrate, and valerate are significantly reduced during VLCD ($n_{intervention}$=18, $n_{control}$=10 participants/timepoint,

FDR Q-values<0.1, two-sided Wilcoxon signed-rank test, downward triangles represent a concentration <10 μg/g). Statistical analysis carried out using linear mixed effects models (LMM) with participant as random effect and Tukey all-pair two-sided comparison unless otherwise noted. In boxplots, the median is represented by the center line with the box representing the 1st and 3rd quartiles, whiskers extend 1.5x the interquartile range with outliers individually plotted.

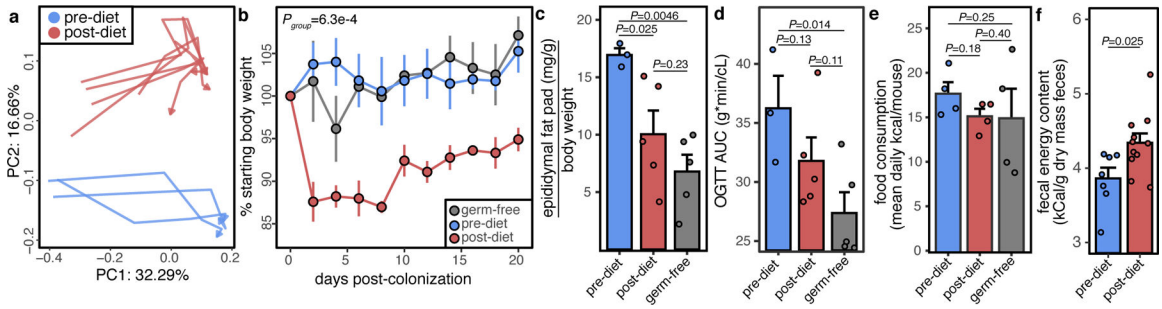

Figure 2. Weight loss and improved metabolic health are transmissible via the gut microbiome.

a, Principal coordinates analysis of unweighted UniFrac distances demonstrates that compositionally distinct communities were established comparing pre- and post-diet recipients across all timepoints with early temporal instability (P_{time}=0.0001 R^2=0.17, P_{group}=0.0001 R^2=0.18, ADONIS). Each mouse is represented as a vector over time terminating at an arrow (day 21). **b,** Change in mouse weight over time demonstrates significant weight loss in post-diet as compared to GF and pre-diet recipients (12.2% [6.5–17.8 95%CI], P=0.0014 LMM). **c,** Decreased adiposity was observed in pre- versus post-diet recipients compared to GF controls (P=0.025). **d,** Pre-diet colonization has a significant effect on oral glucose tolerance as compared to GF controls (P=0.014). **e,** Food consumption did not differ between groups (P=0.63, n=4 time intervals normalized to n_{mice} and interval length in days). **f,** Stool energy density (kCal/g dry mass) is increased in mice colonized with the post-diet microbiome (P=0.025 LMM, collected at days 1 [$n_{pre\text{-}diet}$=2 $n_{post\text{-}diet}$=3 mice], 3 [$n_{pre\text{-}diet}$=2 $n_{post\text{-}diet}$=4 mice], and 7 [$n_{pre\text{-}diet}$=3 $n_{post\text{-}diet}$=4 mice]). Sample numbers for panels a-e are $n_{pre\text{-}diet}$=3, $n_{post\text{-}diet}$=5 mice/timepoint). Data presented as mean±SEM where applicable and statistical analysis carried out using a Kruskal-Wallis test with Dunn's two-sided post-hoc test unless otherwise noted.

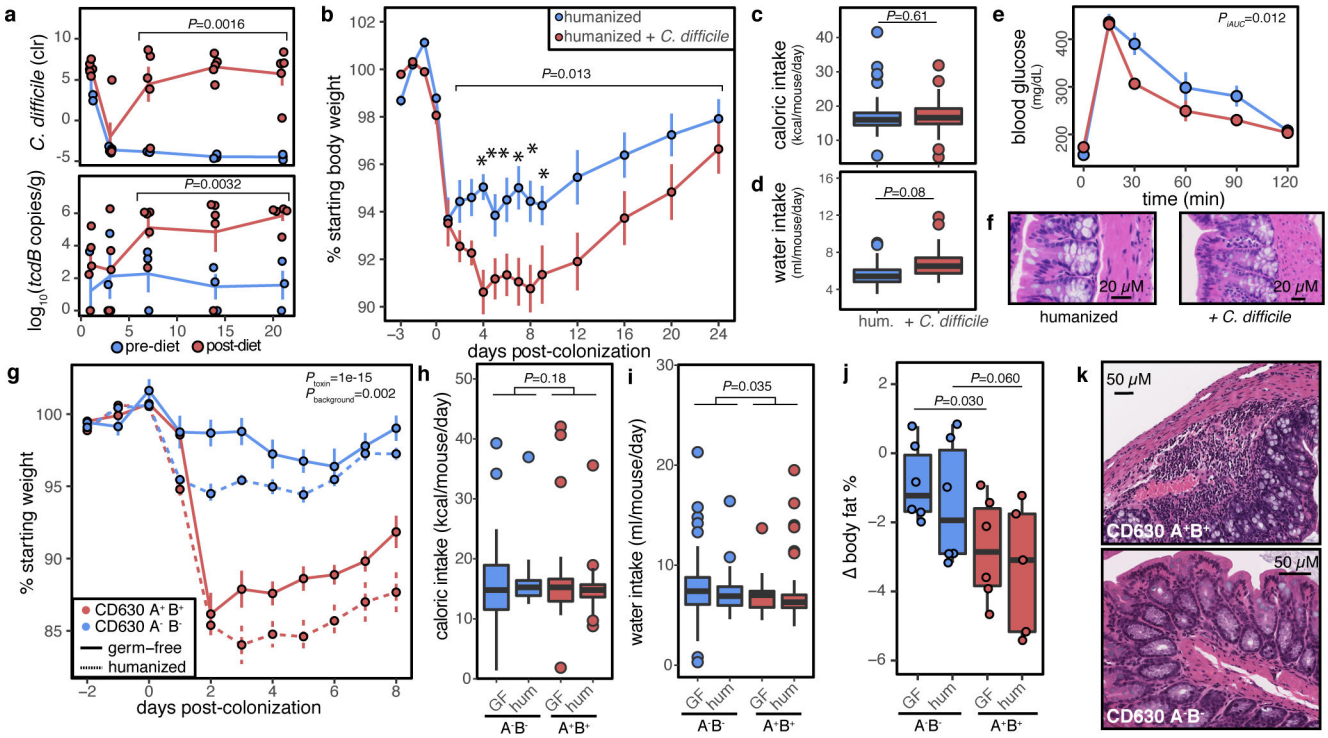

Figure 3. Endogenous *C. difficile* is unrestricted by the post-diet microbiota contributing to weight loss in a toxin-dependent manner.

a, *C. difficile* and *tcdB* are significantly higher in post-diet recipient mice by sequencing (centered log2-ratio) and qPCR (P=0.0016 and P=0.0032 respectively, LMM, $n_{pre\text{-}diet}$=3, $n_{post\text{-}diet}$=5 mice). **b,** Addition of *C. difficile* JBZPo1 spores to a reference donor is sufficient to replicate weight loss versus human-microbiota vehicle control (P=0.013, estimate=3.4% [1.2–5.7 95%CI], LMM 2–24 days post-colonization n=6 mice/group, *P<0.05 two-sided Welch's t-test at individual timepoints. **c,** Daily food consumption (P=0.61, LMM, n=6 mice/group measured over 13 intervals), and **d,** water consumption were not significantly different in *C. difficile*-colonized mice (P=0.08, LMM, n=6 mice/group measured over 14 intervals). **e,** Oral glucose tolerance shows improved response with *C. difficile* (P=0.012 two-sided Welch's t-test of incremental AUC, n=6 mice/group). **f**, Colon tissue does not show gross evidence of colitis (representative images, n=6 mice/group, scoring in Extended Data Fig. 6f). **g,** *C. difficile* induced weight loss in both GF and humanized mice (LMM, n=5–6/group as in Extended Data Figure 8a). **h,** Food consumption is not different between genotypes (P=0.18, LMM), but **i,** water consumption is higher in toxin deficient recipient mice (P=0.035 2.3 mL [0.3–4.3 95%CI], LMM, n=5–6 mice/group/timepoint as in Extended Data Fig. 8a). **j,** Colonization with toxigenic *C. difficile* reduces body fat (P=0.03 GF, P=0.06 humanized, Kruskal-Wallis Test with Dunn's two-sided post-hoc test, n=5–6/group as in Extended Data Figure 8a). **k,** Representative histology demonstrates neutrophil infiltration (Extended Data Fig. 8e). Statistical analysis carried out using linear mixed effects models (LMM) and Tukey two-sided all-pair comparison unless otherwise noted. Error bars represent mean+SEM. In boxplots, the median is represented by the center line with the box representing the 1st and 3rd quartiles, whiskers extend 1.5x the interquartile range with outliers individually plotted.

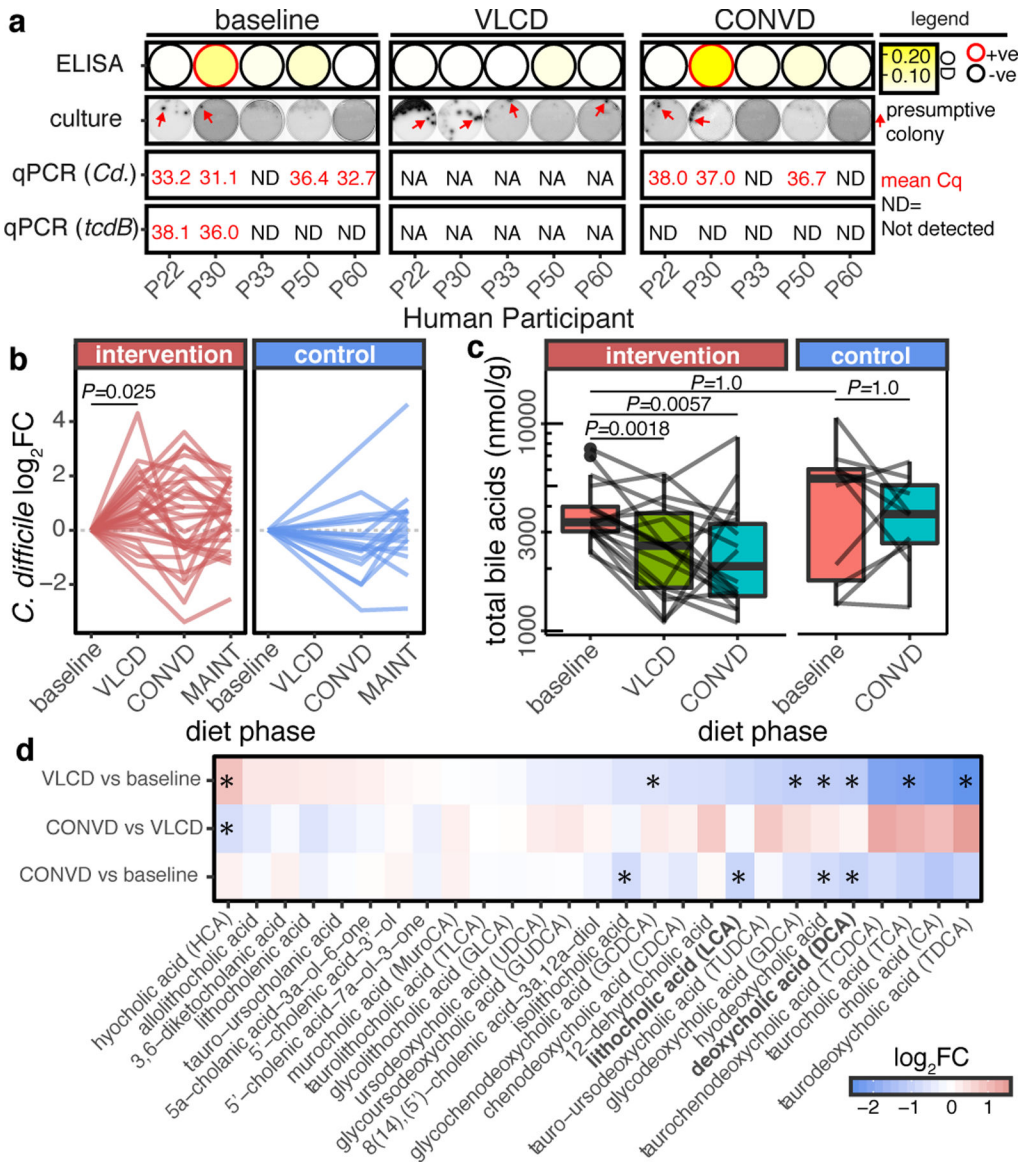

Figure 4. Caloric restriction is associated with an expansion of *C. difficile* and altered bile acid pools.

a, *C. difficile* presence in 5 individuals with the highest weight loss by fecal ELISA for *C. difficile* toxins (TcdA/B), selective and differential culture, and qPCR targeting the *C. difficile* 16S rRNA Gene (*Cd.*) and the toxin B gene (*tcdB*). Normalized optical density (OD) is shown for the ELISA with an OD>0.123 taken as a positive reaction. Culture plates are shown, imaged under long-wave UV, showing the presence of presumptive *C. difficile* colonies (representative indicated with red arrow: fluorescent colonies with ground-glass appearance and filamentous edges, representative plate shown under white light in Extended Data Fig. 9e). Quantitative PCR (qPCR) results are represented as the cycle of quantification (Cq) at which FAM-fluorescence was detected (NA=not assayed). **b,** *C. difficile* abundance, determined from metagenomic sequencing, is significantly increased during VLCD with no other significant contrasts (log_2 fold difference=0.88±0.28 [mean±SE], P=0.025 LMM with Tukey's two-sided all-pair comparison, $n_{intervention}$=29, $n_{control}$=18 participants). **c,** Diet

intervention significantly affects total bile acid pools in human participants ($n_{intervention}$=20, $n_{control}$=10 participants, LMM with Tukey's two-sided all-pair comparison). In panel c, the centerline represents the median with the limits representing the upper and lower quartiles and whiskers extending up to 1.5x the interquartile range with outliers shown as individual points. **d,** Differential bile acid pools in response to diet (n=20, FDR-corrected two-sided Wilcoxon signed-rank test, *FDR Q<0.1).